eLife

Reviewed Preprint
v1 • July 8, 2026
Not revised

For correspondence:
georg.keller@fmi.ch

Competing interests: No competing interests declared

Funding: See page 30

Reviewing editor: Helen Scharfman, Nathan Kline Institute, United States

Electroconvulsive stimulation drives cortical spreading depression dependent immediate early gene expression in mice

Hugo J Ladret[1], Leonardo Lupori[1], Lorenzo Sieni[1,2], Eduard Stroukov[1,2], Takahiro Kanamori[1], Sarah Ulrich[3,4], Else Schneider[3,4], Gunnar Deuring[3,4], Annette B Brühl[3,4], Georg B Keller[1,2]

[1]Friedrich Miescher Institute for Biomedical Research, Basel, Switzerland • [2]Faculty of Science, University of Basel, Basel, Switzerland • [3]Experimental Cognitive and Clinical Affective Neuroscience (ECAN) Laboratory, Department of Clinical Research (DKF), University of Basel, Basel, Switzerland • [4]Center for Affective, Stress and Sleep Disorders, University Psychiatric Clinics (UPK), Basel, Switzerland

eLife Assessment

This study addresses a recent discovery by others that electroconvulsive therapy (ECT) generates seizure activity and spreading depolarization (SD), reflected in large increases in calcium, which can be followed by imaging calcium fluctuations in neurons. This work is **useful**. However, the evidence to show that SD, rather than seizures, confers the neuroplastic and other therapeutic effects of ECT is **incomplete**.

https://doi.org/10.7554/eLife.111896.1.sa3

Abstract

Electroconvulsive therapy (ECT) is a highly effective treatment for several psychiatric disorders, though its biological mechanisms remain unclear. Its therapeutic action has traditionally been attributed to the generalized seizure ECT induces. However, this view is challenged by the recent finding that electroconvulsive stimulation (ECS) can trigger a cortical spreading depression (CSD). Because CSD triggers massive intracellular molecular changes, we hypothesized that it could be a key mediator of ECT's therapeutic, plasticity-inducing effects. We observed similar neuronal oscillations following ECS in mice and patients undergoing ECT. We show that CSD drives increased expression of the immediate early gene Fos, a key marker of neuronal plasticity, and is associated with factors that predict positive ECT therapeutic outcome. Our results suggest that the therapeutic efficacy of ECT may be mediated by CSD. This challenges the seizure-centric model and implies that CSD, a currently unmonitored neurophysiological event, may serve as a more relevant biomarker for predicting and optimizing therapeutic outcomes of ECT.

Introduction

Electroconvulsive therapy (ECT) is one of the most potent and rapidly acting interventions in clinical psychiatry. It demonstrates substantial efficacy in treating severe and often treatment-resistant conditions, including major depressive disorder (Trifu et al., 2021), bipolar disorders (Tor et al., 2021), catatonia (Perugi et al., 2017), mania (Martin et al., 2025) and schizophrenia (Grover et al., 2019). ECT frequently achieves positive therapeutic outcomes in terms of remission rates and speed of response that surpass standard pharmacotherapies, making it indispensable in urgent clinical situations such as high suicide risk or severe catatonia (Baghai and Möller, 2008). ECT is also one of the few treatment options available to drug-resistant

patients (Haddad and Correll, 2018). Despite its established clinical utility and decades of refinement aimed at enhancing safety and tolerability, the fundamental neurobiological mechanisms driving ECT's therapeutic effects remain poorly understood.

There is a multitude of biomarkers affected by ECT that could underlie its mode of action as a psychiatric treatment (Singh and Kar, 2017). These include, non-exhaustively, the modulation of various neurotransmitter systems (Baldinger et al., 2014), alterations in regional cerebral blood flow (Takano et al., 2011) and metabolism (McCormick et al., 2007), changes in functional brain network connectivity (Ulrich et al., 2025), and the promotion of neuroplasticity (Bouckaert et al., 2014; Chen et al., 2018; Joshi et al., 2016). Understanding how these effects contribute to therapeutic outcomes is a significant challenge. We suspect that a critical gap in our knowledge lies in the early cascade of events triggered by an ECT treatment.

ECT, as it is used today, is targeted at the induction of a controlled seizure under general anesthesia and muscle relaxation through an electroconvulsive stimulation (ECS). Import to note here is that the term seizure likely refers to a different neuronal event in the context of ECT and epilepsy. In modern practice, ECS triggered seizures are highly synchronized brain-wide oscillations, which typically follow a three-phase progression (Brumback and Staton, 1982) consisting of an immediate 14-22 Hz activity (phase I), which evolves into arhythmic poly-spike patterns (phase II) and is then rapidly, within seconds, followed by a sustained low-frequency oscillation at 2-4 Hz (phase III). Phase III oscillations often occur without any ictal spikes that are characteristic of epileptic seizures (Brumback and Staton, 1982) and share limited similarities only with the late phase of seizures observed in epilepsy (Pottkämper et al., 2021). The phase III oscillation is referred to as seizure in the ECT literature. Illustrating the difference between what is referred to as a seizure in the ECT literature and what is referred to as a seizure in the epilepsy literature is also the fact that the post-seizure neuronal silencing of activity is a marker of treatment success in ECS, while it is associated with sudden unexpected death in epilepsy (Krystal et al., 1995; Sowers et al., 2013), and the finding that antiepileptics do not block ECS-triggered seizures (Cinderella et al., 2022). To try to disambiguate this, we will refer to the ECS induced seizure as phase III oscillation in the description of our results, but consistent with previous usage as seizure when talking about prior ECT work.

Historically, the generalized ECS induced seizure was considered to be the essential therapeutic component of the treatment (Accornero, 1988; Ulett et al., 1956). However, the occurrence and properties of seizures are only partially predictive of therapeutic outcomes (Perera et al., 2004; Sackeim et al., 1991). Similarly, the clinical efficacy of alternative stimulation methods, such as low amplitude ECT or magnetic seizure therapy, demonstrates that robust outcomes can be achieved with lower field strengths (Peterchev et al., 2015). This discrepancy suggests that electric field strength is unlikely to be the primary determinant of therapeutic success (Deng et al., 2024), indicating that ECT's efficacy hinges on biological mechanisms beyond the mere presence of a seizure or the magnitude of the electrical stimulus.

A secondary neurophysiological event frequently triggered by seizures is cortical spreading depression (CSD). It has been speculated that CSD is an endogenous mechanism of the brain used for seizure termination (Dreier et al., 2012; Kelly et al., 1999). A CSD can also be triggered by direct electrical stimulation of the cortex (Fregni et al., 2007; Leao, 1944), and, consistent with this, recent evidence revealed the existence of CSD-like calcium events following ECS in mice and likely following ECT in patients (Rosenthal et al., 2025). This discovery necessitates a critical re-evaluation of the traditional seizure-centric view of the effects of ECT. The profound neurophysiological disruption inherent to CSD may potentially act as a trigger for several of the neurobiological alterations driven by ECT.

CSD is characterized as a slowly propagating wave (typically 2–5 mm/min) of near-complete, and sustained depolarization affecting both neurons and glial cells (Seidel et al., 2016). This wave of intense depolarization is invariably followed by a period of marked suppression of spontaneous and evoked electrophysiological activity that lasts several minutes and can persist for up to an hour (Sawant-Pokam et al., 2017). The wavefront of the CSD is a massive transmembrane ionic flux (Somjen, 2001) that is accompanied by cellular swelling due to water movement, blood flow

changes resulting in local hypoxia, and structural changes to dendritic processes (Takano et al., 2007). A CSD can be triggered by a large efflux of potassium ions into the extracellular space (Brinley et al., 1960) that causes a positive feedback loop via glutamate release, which propagates the wavefront through the activation of NMDA receptors (Zhou et al., 2013). Concurrently, there is an influx of sodium, chloride and calcium ions into cells (Pietrobon and Moskowitz, 2014). Disturbed calcium signaling is associated with a host of neuropsychiatric disorders treated by ECT (Nanou and Catterall, 2018), which makes CSD driven calcium influxes a likely key contributor to neuronal plasticity effects driven by ECT (Dehbandi et al., 2008; Wernsmann et al., 2006).

Here, we sought to characterize the specific calcium dynamics during ECS-induced CSD, hypothesizing they might underlie the plasticity-relevant effect of ECT. Consistent with previous work (Rosenthal et al., 2025), we observed a slow travelling calcium event that appeared to be a CSD. We found that the characteristics of this calcium event were consistent with being a CSD, and that it accounted for the ECS driven Fos expression, a marker of neuronal plasticity in the cortex (Mahringer et al., 2022, 2019). Furthermore, we show that EEG metrics known to predict positive therapeutic outcomes of ECT are correlated with the occurrence of CSD in mice. Our findings support the hypothesis that CSD, rather than the seizure itself, is the primary driver of ECS driven plasticity and, by extension, the therapeutic benefits of ECT.

Results

ECS triggers similar neuronal oscillations in both mice and humans

We first asked how well ECS in mice recapitulates EEG signatures of ECS in humans. To do this, we measured neuronal responses following ECS in mouse dorsal cortex, using concurrent widefield calcium imaging and EEG recordings (Methods). We expressed a genetically encoded calcium indicator brain-wide by retroorbital deposit of an AAV-PHP.eB-Ef1α-GCaMP6s-WPRE and performed concurrent EEG recordings using a semitransparent 30-channel EEG electrode (Figure 1A). During ECS, mice were anesthetized with isoflurane (2%) and myorelaxed with succinylcholine chloride (1mg/kg). ECS was delivered through biauricular electrodes using a commercial ECS unit. Stimulation parameters were set within a range that reliably evoked tonic-clonic seizures in mice (Methods).

Across the parameter range used, ECS triggered an immediate and brief calcium response across the entire dorsal cortex (Figure S1A). The response onset occurred with a latency of less than 10 ms (within the first frame after stimulation at 100 Hz acquisition), and calcium activity continued to increase until the end of the ECS (Figure S1B). In the EEG data (Figure S1C) we were blind to this direct response, as we disconnected the EEG from the data acquisition system during ECS to prevent electrical arcing between electrodes (Methods). We speculate that the direct ECS response observed in calcium imaging is driven by spiking activity in the cortical neurons, given that the electrical field generated by the ECS is several times higher than the neuronal activation threshold (Deng et al., 2011). Following the direct calcium response to ECS, mean calcium activity decreased and returned to baseline only slowly (Figure S1B).

The combined median duration of phases I and II is 9 s (Hogan et al., 2019). Consistent with this, we observed a phase III slow oscillation in the delta to low theta range (1 to 5 Hz) in mice that emerged about 10 s after the ECS, both in calcium activity and EEG recordings (Figure 1B-C, S2). This oscillation was strikingly similar to that observed in patients undergoing ECT (Figure 1D-E) (Stuiver et al., 2026), and was present in the EEG recording of all patients analyzed here. Given that ECT stimulation parameters are chosen to increase the likelihood of phase III oscillations, which in turn are used as a biomarker for treatment outcome (Sackeim et al., 1991), this is perhaps not surprising.

The oscillation followed a similar pattern in both mice and patients and typically exhibited a strong sinusoidal shape in the early stage that desynchronized over time (Figure 1F). In mice, the oscillations lasted 42.3 ± 11.9 s (mean ± std), and we found no evidence of a difference in oscillation duration between mice and patients (Figure 1G). These values are consistent with

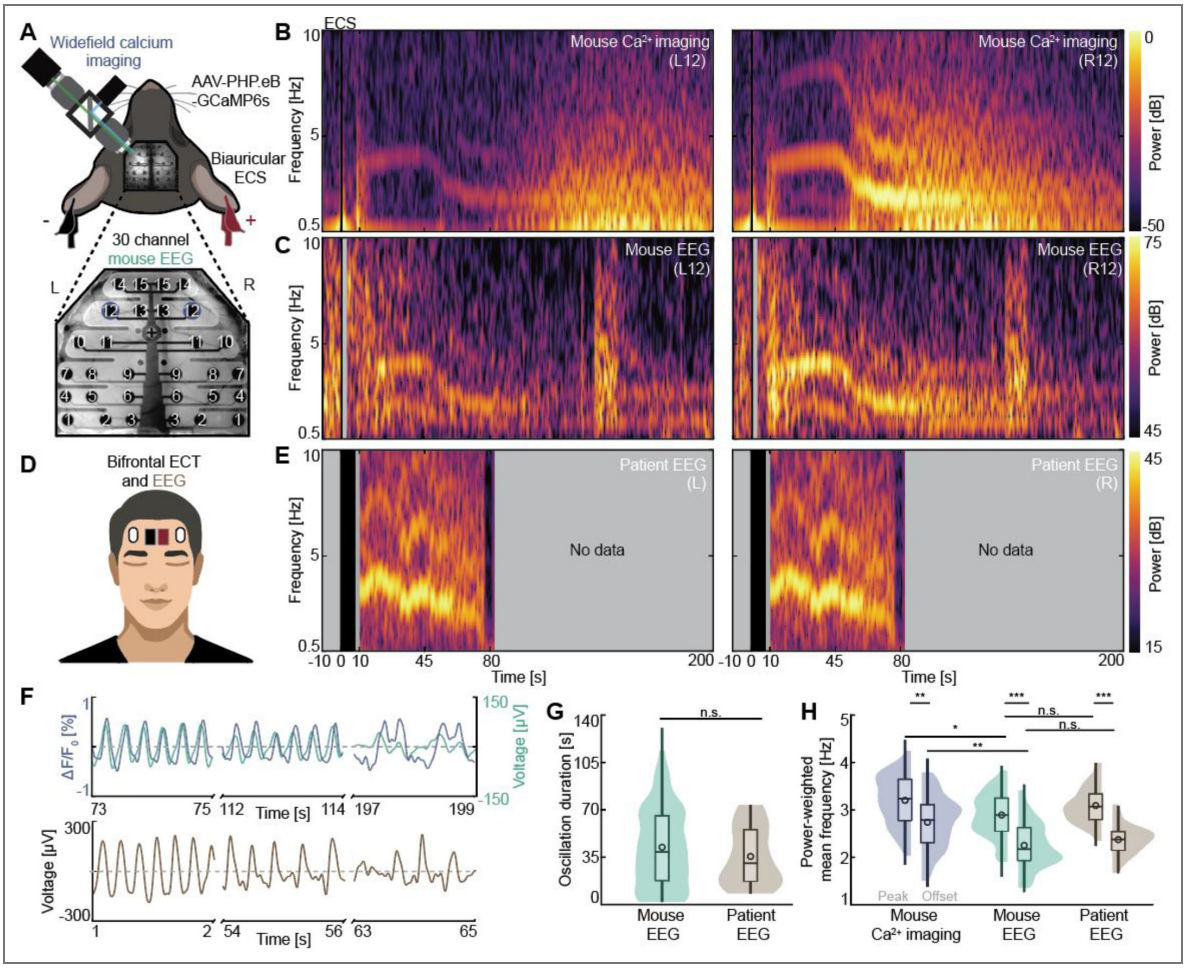

Figure 1. Electroconvulsive stimulation (ECS) triggers similar slow neuronal oscillations in mice and humans.

(A)Top: Schematic of mouse ECS setup. We performed concurrent widefield calcium imaging and EEG in the mouse dorsal cortex during biauricular ECS. Bottom: Layout of the EEG probe. (B)Spectrograms of two widefield calcium imaging ROIs surrounding EEG electrodes L12 and R12 (as highlighted in **A**). Duration of the ECS is marked by a black bar. (C)Spectrograms of the EEG recorded concurrently with the widefield calcium data in **C**. Time during which EEG is not recorded due to a stimulation artifact is marked by gray shading. (D)Schematic of patient ECS setup. EEG recordings were performed using two frontal electrodes after bifrontal ECS in patients. (E)Spectrograms of EEG recorded following ECT in a patient. Patient EEG recordings are started following ECS and terminated when the oscillation stops. Gray shading marks times without EEG recording. (F)Top: Oscillations observed in early, mid, and late phases after ECS in an example mouse widefield calcium ROI (blue) and in the concurrently recorded EEG (green). Bottom: Oscillations observed in an example patient EEG recording. (G)Oscillation duration for mouse and patient EEG recordings. The central box represents the interquartile range (IQR), spanning from the first (Q_1) to the third (Q_3) quartiles. Whiskers extend to data points not considered outliers (Methods). A central horizontal line indicates the median and an open circle the mean of the data distribution. (H)Power-weighted mean frequency at peak and offset of oscillations for mouse widefield, mouse EEG and patient EEG recordings. Here and elsewhere: n.s.: not significant, *: $p < 0.05$, **: $p < 0.01$, ***: $p < 0.001$. See Table S1 for all information on statistical testing.

previous estimates of the duration of phase III oscillations in patients (Hogan et al., 2019). Interestingly, the frequencies of the oscillations were also very similar in mice and patient EEG, and both tended to decrease with time (Figure 1H). The estimate of the oscillation frequency in the mouse calcium imaging data was systematically higher relative to the concurrent EEG data (Figure 1H) but exhibited the same decreasing trend. We suspect this difference is driven by differential contributions to the two signals from non-oscillation related neuronal activity and noise sources.

ECS can trigger a travelling calcium event

We found that ECS could also trigger a travelling calcium event, as previously described (Rosenthal et al., 2025). To monitor the propagation of these events, we recorded the calcium activity across the entire dorsal cortex for 3 to 5 minutes following ECS (Figure 2A). They manifested as a significant increase in calcium fluorescence that propagated across the dorsal cortex (Figure 2B) at a speed of 0.083 ± 0.009 mm/s (mean ± std) (Figure 2C), consistent with previously reported CSD propagation speeds in mice (Enger et al., 2015). Calcium events exhibited maximum fluorescence intensities that exceeded even those observed during the direct ECS response (Figure 2D). Once initiated, these events spread across an entire dorsal cortex hemisphere over the course of several minutes (Figure 2E). In line with the refractory dynamics of CSD, the event exhibited a non-repeating trajectory, traversing each part of dorsal cortex only once. The lateralization of the events exhibited a certain stochasticity and calcium events were not always symmetrically present in both hemispheres. We frequently observed cases in which the events were unilateral and constrained to only left or right cortical hemispheres (Figure 2F-G).

In about one third of cases, calcium events appeared bilaterally, while in the remaining two thirds the events were confined to one hemisphere only (Figure 3A, Video S1). The majority of unilateral events occurred in the right hemisphere, and across all events, most first appeared on the right edge of the cranial window (Figure 3B). This right hemisphere bias was likely driven by the ECS polarity, as we always placed the positive pole of stimulation on the right ear (Figure 1A). Calcium events were the only type of response to ECS that occurred unilaterally (Figure 3C). While all calcium events co-occurred with oscillations, just over half of the oscillations were accompanied by a calcium event (Figure 3D). The likelihood of triggering a calcium event has been shown to be a function of the stimulation current and frequency used of the ECS (Rosenthal et al., 2025). To investigate how the stimulation parameters control the appearance of oscillations and calcium events, we tested stimulation frequencies between 25 and 100 Hz and stimulation currents between 15 and 75 mA for a total charge delivery of between 0.187 and 3.750 mC. With most combinations of parameters, we observed a non-zero likelihood of triggering a phase III oscillation (Figure 3E). The threshold for triggering calcium events was systematically higher and appeared to be a function of both stimulation frequency and current (Figure 3E). Based on this, we hypothesized that total charge delivery might be a good predictor of the occurrence of calcium events. A linear regression of total stimulation charge against the likelihood of triggering a calcium event showed a significant correlation (Figure 3F). Stimulation frequency and stimulation current also exhibited a positive but nonsignificant correlation with the likelihood of triggering a calcium event (Figure S3A). A multivariate linear regression confirmed that the interaction term of current and frequency was significant and non-zero (0.015 % / (mA Hz)). We found a similar relationship between the total stimulation charge and the probability of triggering a phase III oscillation (Figure 3G, S3B). Consistent with the hypothesis that the calcium event exhibits all-or-none dynamics, we found no evidence of changes in propagation speed, total duration, or delay to onset of calcium events as a function of total stimulation charge (Figure S3C-E). We also observed that the total ECS charge correlated with the intensity of the direct ECS response (Figure S4A). This direct response, in turn, predicted the hemisphere of the calcium event in 75% of the unilateral cases (Figure S4B), supporting our hypothesis that the ECS stimulation parameters can control the occurrence of calcium events.

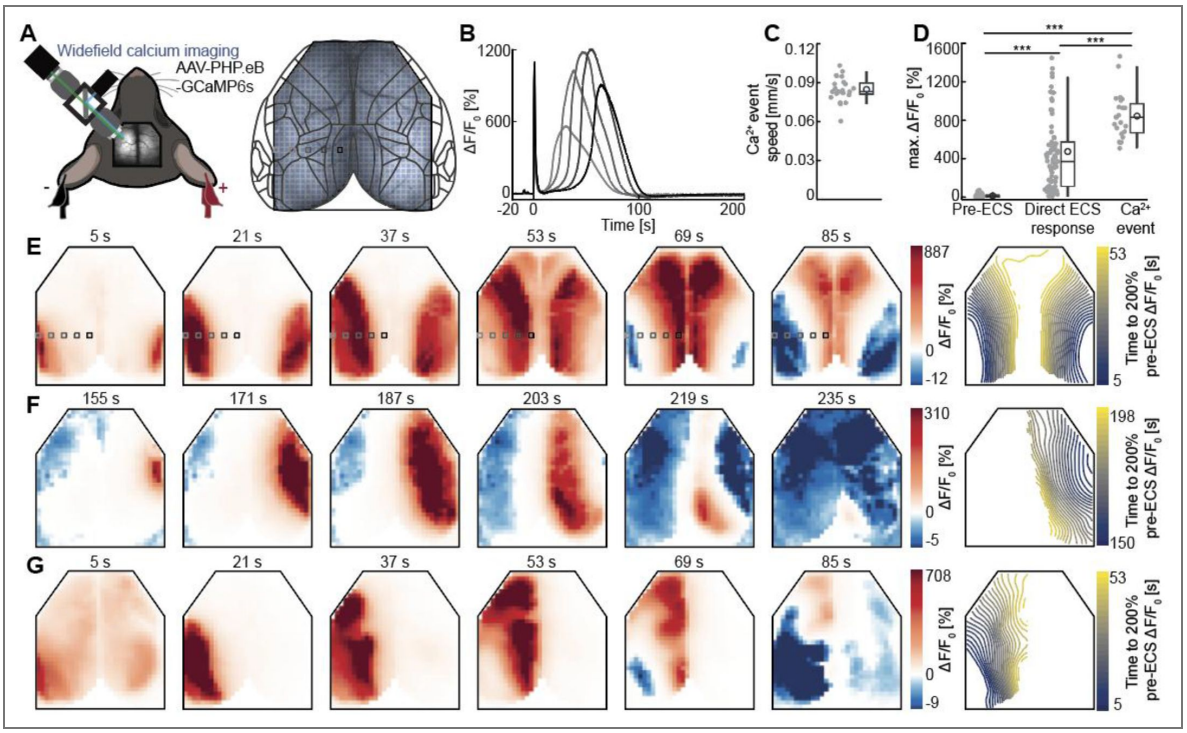

Figure 2. ECS can trigger a travelling calcium event.

(A)Left: Schematic of mouse ECS setup without concurrent EEG recordings. Right: Widefield recordings of mouse dorsal cortex were parcellated into 818 ROIs, each of which was assigned to a cortical region according to the Allen Brain Atlas taxonomy. The ROIs highlighted correspond to the calcium activity shown in **B** and **E**. (B)Example of calcium activity in ROIs highlighted in **A** during the traversal of a calcium event. (C)Propagation speed of calcium events (Methods). Each data point is the median speed across one calcium event. (D)Maximum calcium activity throughout the dorsal cortex during pre-ECS, direct ECS response and calcium event periods. Two direct ECS responses are outside the plot range and not shown (1707 % and 2374 % ΔF/F0). (E)Left: Low-passed (< 0.5 Hz) calcium activity during an example ECS session triggering calcium event over both hemispheres. Each panel shows the average calcium activity over a 10 ms window starting at the time indicated above the panel. Right: Isochrones (spaced at two seconds increments) indicating the time at which each region reaches 200% of its baseline fluorescence. (F)As in **E**, but for a unilateral calcium event over the right hemisphere following a 150 s delay post-ECS. (G)As in **E**, but for a unilateral calcium event over the left hemisphere.

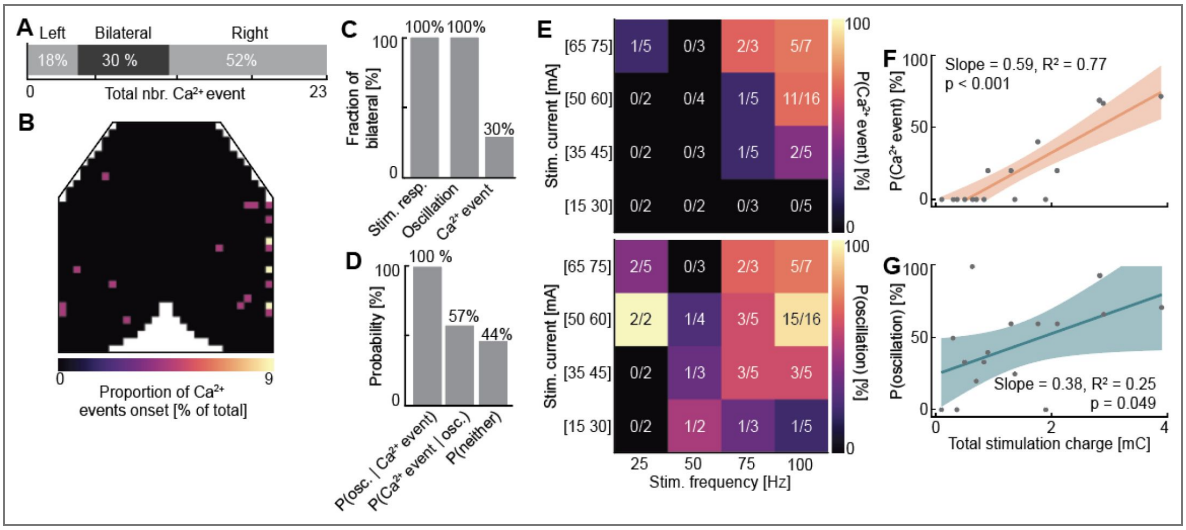

Figure 3. Calcium events are triggered preferentially by higher total ECS charge.

(A)Probability distribution of the laterality of calcium events. (B)Spatial distribution of calcium events detection sites. For bilateral calcium events, only the hemisphere where the calcium event was detected earliest is considered as the detection site. (C)Fraction of stimulation responses, oscillations and calcium events that were bilateral. (D)Probability of oscillations being observed if a calcium event is triggered (P(osc. | calcium event)), of a calcium event being observed if an oscillation is triggered (P(calcium event | osc.)), and of neither being observed (P(neither)). (E)ECS parameter map of the likelihood of triggering a calcium event (top) or an oscillation (bottom). (F)Probability of triggering a calcium event as a function of total ECS stimulation charge. The solid line represents the linear fit of the data; the shaded region represents 95% confidence interval on the fit. (G)As in **E**, but for the probability of triggering an oscillation.

The calcium event exhibits hallmark features of CSD

The mode of propagation, speed and fluorescence intensity support the hypothesis that the travelling calcium event is a CSD. This has already been speculated previously (Rosenthal et al., 2025), and makes a number of directly testable predictions. First, a CSD changes the local ionic homeostasis and is accompanied by hemodynamic constriction (Takano et al., 2011). To test for hemodynamic effects triggered by ECS, we performed widefield imaging experiments in a cohort of mice in which we expressed enhanced green fluorescent protein using an AAV (EGFP,AAV-PHP.eB-Ef1α-EGFP-WPRE). In widefield imaging, the EGFP fluorescence signal depends on pH and overlying blood volume. The latter is a phenomenon called hemodynamic occlusion, whereby decreased blood vessel diameter increases the EGFP signal (Ma et al., 2016; Yogesh et al., 2025). During the ECS, we observed an immediate increase in the EGFP signal that lasted for a couple of seconds and is consistent with acute vasoconstriction (Figure S5A). We also observed travelling signals in the EGFP recordings with spatial and temporal characteristics that resembled the calcium event (Figure S5B). The amplitude of these events was smaller than that observed in calcium imaging (Figure S5C), but they propagated at a speed that did not differ significantly from that observed in calcium events (0.096 ± 0.02 mm/s, Figure S5D). This would be consistent with either vasoconstriction or an increase in intracellular pH. CSD is associated with vasoconstriction (Takano et al., 2007), but typically only a brief alkalization over the course of seconds followed by a more prolonged acidification of the intracellular domain over the course of minutes (Sun et al., 2011). However, given that an estimated alkalization of less than 0.5 in pH, would translate to less than a 10% $\Delta F/F_0$ change in EGFP fluorescence (Kneen et al., 1998), we suspect most of the change we observe is driven by hemodynamics.

A second feature of CSD is the propagation through extracellular diffusion (Enger et al., 2015), rather than through electrical activity. Increases in intracellular calcium levels in neurons are typically associated with increases in spiking activity. A CSD, however, is associated only with brief increases in spiking activity at the onset (Herreras et al., 1994; Nasretdinov et al., 2023). To visualize the propagation of the calcium event in the tissue, we used two-photon microscopy to observe the wavefront at cellular resolution. We expressed a genetically encoded calcium indicator (AAV2/9-Ef1α-GCaMP6f-WPRE) in visual cortex and measured responses to ECS in layer 2/3 neurons (Figure 4A, Video S2). Consistent with a diffusion-limited process, we found that the calcium event was a sharp wavefront of significant increase in fluorescence, propagating across the entire field of view (Figure 4B) at a speed of 0.079 ± 0.0174 mm/s (mean ± std). This aligns with our speed estimates based on widefield calcium imaging. Combined with the lack of propagation along inter-hemispheric or other known anatomical projections (Figure 2E-G), this supports the idea that the calcium events are propagating through a diffusion-limited process, rather than synaptic activity, consistent with a CSD.

A third hallmark feature of CSD is its preferential propagation through superficial cortical layers (Stafstrom, 2020; Zakharov et al., 2019). To investigate this, we implanted a micro-prism in the cortex, enabling simultaneous imaging across all cortical layers (Figure 4C, Video S3). We found that the calcium event first spread in superficial layers 2/3 and 4, and only later reached deeper layers 5 and 6 (Figure 4D). Calcium event response in superficial layers preceded those in deep layers by 6.9 ± 1.3 s (mean ± std) (Figure 4E-F). While both somata and neuropil showed a sharp calcium fluorescence increase at the wave front, calcium decay kinetics were more heterogeneous. Calcium fluorescence in the neuropil gradually returned to baseline over the course of about 100 s. Most somata followed this time course, but a subset of them exhibited a progressive increase in fluorescence (Figure 4G), likely reflecting a slow accumulation of somatic calcium. This resulted in a population average fluorescence decrease that was significantly faster in the neuropil than in the somata (Figure 4H-I). The somata with increasing post-calcium event fluorescence made up about 35% of the total somatic population (Figure 4J). This heterogeneous response pattern is a characteristic of CSD, and is hypothesized to be linked to the variable capacity of individual neurons to recover from CSD-induced oxidative stress (Enger et al., 2015). Overall, these results strongly support the hypothesis that the ECS triggered calcium events are indeed CSD.

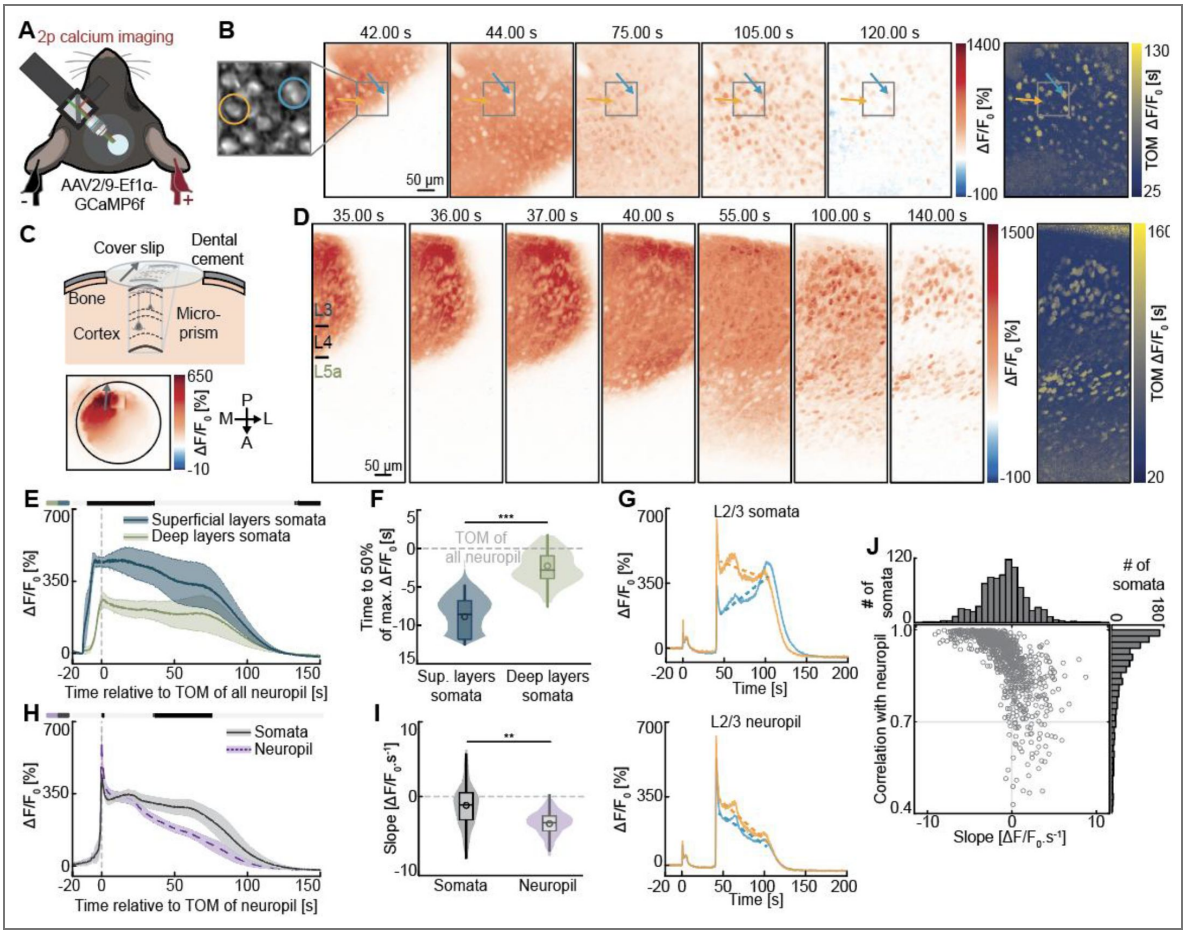

Figure 4. Calcium events first spread in supragranular layers and elicit long-lasting calcium increase in cells.

(A)Schematic of the experimental setup. We performed two-photon (2p) calcium imaging in the right primary visual cortex during ECS. (B)2p calcium activity during an example ECS session triggering a calcium event. Time of maximum (TOM) is shown on the right. Each panel shows the average calcium fluorescence over a 500 ms window starting at the time indicated above the panel. Gray inset highlights two example somata whose calcium signals are shown in **G**. (C)Top: Schematic of the micro-prism implanted below the imaging window to allow for simultaneous recording in all cortical layers (see Methods). Bottom: Widefield imaging of the implant 18 seconds after ECS, confirming the prism does not obstruct the calcium event propagation. A gray arrow indicates the orientation of the prism. (D)As in **B**, but imaged through a prism implant. Cortical layers 3, 4, and 5a (L3, L4, L5a) are defined based on soma densities (Methods). (E)Calcium fluorescence of superficial (blue) and deep (green) layers somata during calcium events, aligned to the time of maximum of all neuropil (Methods). Lines represent the hierarchical bootstrap estimates of the mean value for each time bin. Here and elsewhere, shading around the mean is one standard deviation of the bootstrap distribution at each time bin. Response curves are compared for each time bin: in the horizontal bars above the plot, black marks time bins where $p<0.05$ and gray mark time bins where $p>0.05$. (F)Time of 50% of maximum activity for superficial and deep layers somata during calcium events. (G)Top: Calcium fluorescence from the two example somata in **B**. Bottom: Calcium fluorescence from the neuropil surrounding these somata. Fitted slopes during the 60 seconds following calcium event onset are shown as dashed lines. (H)Calcium fluorescence of somata (dark gray) and neuropil (purple) in all layers during calcium events. Each soma is aligned to the time of maximum of the neuropil. (I)Distribution of the fitted slopes for cells and neuropil during the 60 seconds following calcium events. (J)Scatter plot of fitted slopes and correlation of cells with their neuropil. Top and right histograms are marginal distributions over slopes and correlations, respectively.

Calcium events, not ECS, drives Fos expression

If those calcium events are CSD, then they should cause neuronal plasticity (Faraguna et al., 2010; Li et al., 2012). To begin testing this hypothesis, we quantified the ECS driven expression of the Fos protein, the product of an immediate early gene that is a marker of functional plasticity in cortex and hippocampus (Mahringer et al., 2022, 2019). We again performed widefield calcium imaging of ECS responses and allowed one hour of recovery post-ECS for Fos expression (Methods). Brain tissue was then processed for Fos immunohistochemistry. We found that ECS drove strong Fos expression in a variety of brain areas, including the cortex (Figure 5A). To determine whether it was the direct electrical response to the ECS or the calcium event that drove Fos expression, we again took advantage of the occurrence of unilateral calcium events (Figure 5B). In these cases, we could directly compare Fos expression in the hemisphere that exhibited a calcium event to that in the hemisphere that did not. Remarkably, hemispheres without a calcium event showed Fos levels not statistically different from sham-treated mice, and the ECS driven increase in Fos expression could be fully explained by the calcium event (Figure 5C). This supports the hypothesis that calcium events, which are likely CSD, are the primary driver of neuronal plasticity following ECS.

The occurrence of calcium events correlates with EEG metrics predicting positive ECT therapeutic outcomes

Given that calcium events accounted entirely for the expression of Fos, we speculated that they may also be the driver of the positive therapeutic outcomes of ECT. A first testable prediction of this hypothesis is that EEG responses to ECS that correlate with positive therapeutic outcomes should also correlate with the occurrence of calcium events. While EEG responses are only partially predictive of clinical improvement following ECT (Krystal and Weiner, 1994), there are several EEG metrics that correlate with positive therapeutic outcomes. For the phase III oscillation, an increased amplitude (Perera et al., 2004), a longer duration (Gillving et al., 2024), a higher post oscillation suppression index (Kimball et al., 2009; Nobler et al., 1993), and higher interhemispheric coherence (Grözinger et al., 2013), for example, are indicators of a favorable patient response to ECT (Francis-Taylor et al., 2020).

To address this, we investigated whether these EEG metrics correlated with the occurrence of a calcium event, by comparing EEG data from recordings without and with calcium events (Figure 6A-B). We found that the mid-phase III oscillation amplitude was significantly higher in hemispheres where a calcium event occurred compared to the unaffected contralateral hemisphere or to ECS where neither hemisphere showed a calcium event (Figure 6C). Both the oscillation duration and postictal suppression index (Figure 6D-E) were increased in ECS triggering a calcium event, but we found no evidence that the laterality of the calcium event (ipsi- vs. contralateral) influenced these two metrics. This absence of hemisphere specificity would be consistent with the observation of a tight coupling of onsets and offsets of phase III oscillations across the hemispheres (Brumback and Staton, 1982). In the case of inter-hemispheric coherence of the EEG signals, we found no evidence of an influence of the calcium event (Figure 6F). These results led us to speculate that calcium events may serve as a central mechanistic driver of the therapeutic efficacy of ECT.

Discussion

Here, we sought to characterize the neuronal response to ECS, focusing on a calcium event that shows hallmark features of a CSD. We demonstrate that these events correlate with prognostic EEG markers of ECT treatment outcomes and induce the expression of Fos, a key indicator of neuronal plasticity. Based on our results, we propose that CSD may be a more relevant biomarker than the phase III oscillation to explain the therapeutic effects of ECT.

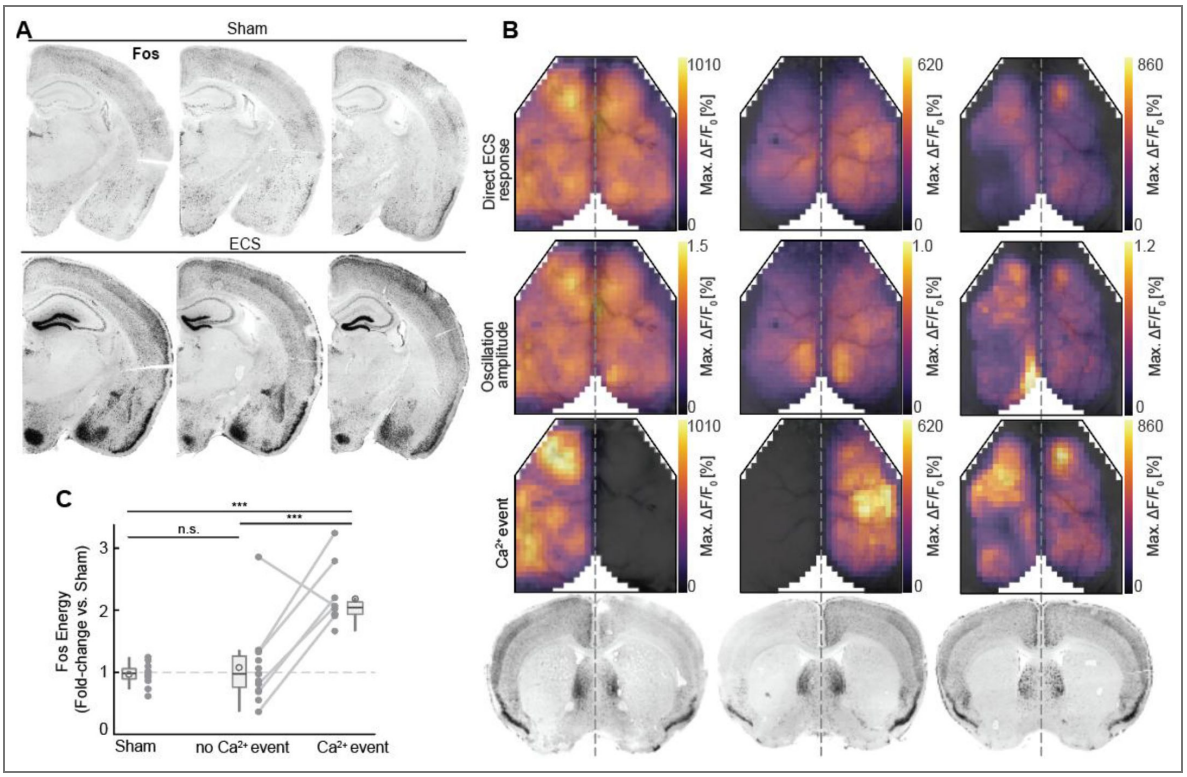

Figure 5. The ECS triggered increase in Fos expression in cortex is driven by the calcium event.

(A)Example of coronal brain sections stained for Fos from three sham ECS (top) and three ECS-treated (bottom) mice. (B)Maximum calcium fluorescence during direct ECS response (first row), the amplitude of the ECS induced oscillation (second row), and the peak fluorescence to illustrate the presence or absence of a calcium event (third row). From left to right, data from three example mice that had unilateral left, unilateral right, and bilateral calcium events, respectively. The bottom row shows corresponding coronal sections from the same brains, stained for Fos expression. (C)Quantification of the Fos throughout the entire cortex, expressed as a fold change for an entire hemisphere normalized to sham mice (see Methods). Paired hemispheres (experiments in which ECS triggered a bilateral direct ECS response and oscillation followed by a unilateral calcium event) are linked by a line. Thus, the calcium event, not the direct ECS response or the phase III oscillation, is the correlate of Fos expression.

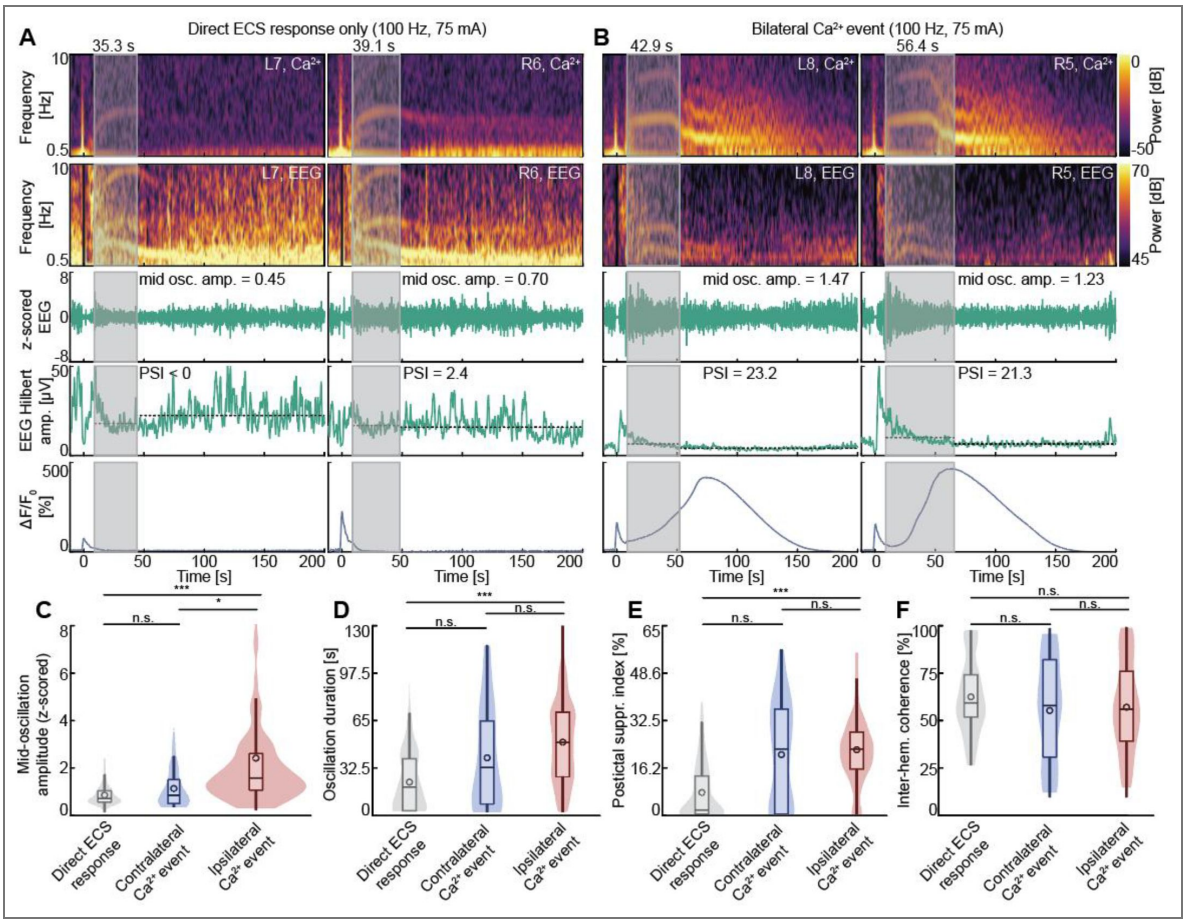

Figure 6. Calcium events are associated with ictal EEG metrics that predict clinical ECT efficacy.

(A)Example of an ECS session triggering a direct ECS response followed by a slow oscillation. Data is shown for two example electrodes. A gray transparent square indicates the duration of the oscillation. First row: Calcium imaging spectrogram of the ROI surrounding the electrode. Second row: EEG signal spectrogram of the electrode. Third row: z-scored EEG signal in the 1-5 Hz band to visualize the oscillation amplitude. Fourth row: EEG Hilbert amplitude in the 1-30Hz band, with dashed lines indicating the mean amplitudes during and after the oscillations used to compute the postictal suppression index (PSI). Fifth row: Calcium imaging fluorescence, low-passed below 0.5 Hz. (B)As in **A**, with identical ECS stimulation parameters, but for an ECS session triggering a direct ECS response followed by a bilateral calcium event. (C)Mid-oscillation amplitude for each electrode during ECS sessions triggering only direct ECS response (gray), ECS sessions triggering a unilateral calcium event over the contralateral hemisphere (blue) and ECS sessions triggering a calcium event on the ipsilateral hemisphere (red, either unilateral or bilateral calcium event). See Methods for the details on the ictal EEG metrics definitions. (D)As in **C**, but for the oscillation duration. (E)As in **C**, but for the postictal suppression index. (F)As in **C**, but for the inter-hemispheric coherence of the EEG signal.

Limitations

There are two key limitations that constrain the interpretation of our results, and that will need to be addressed in future research:

1. We have no direct evidence that patients also have ECT-induced CSD. Patients are typically monitored with two-channel EEG to determine whether ECT has induced a phase III oscillation (Francis-Taylor et al., 2020), but these measurements are currently not sufficient to detect CSD. One simple way to modify the current clinical routine measurements would be to perform direct current (DC) EEG recordings with a higher channel count. CSD results in characteristic DC shifts in the EEG response (Hartings, 2016). While detecting stochastically-occurring CSD signatures in EEG recordings of awake subjects is difficult (Lauritzen et al., 2011), this would likely be facilitated in the context of ECT by the known timing of the triggering stimulus and the elimination of movement artifacts via anesthesia and myorelaxation (Hofmeijer et al., 2018). Alternatively, given that the CSD triggers a strong hemodynamic change (Figure S5) (Hadjikhani et al., 2001), blood-oxygenation level dependent imaging techniques might be able to detect a CSD. There is already evidence of hemodynamic changes induced by ECT in patients (Rosenthal et al., 2025).
2. Our conclusion that the CSD is the primary driver of plasticity is based on its role in driving Fos expression, an early marker of cortical plasticity (Mahringer et al., 2022, 2019). We cannot rule out the possibility that the seizure induced by ECS drives Fos independent plasticity pathways that also contribute to therapeutic outcomes. Like CSD, seizures are neuronal events characterized by supra-physiological excitability that trigger neuronal plasticity (Scharfman, 2002). While knocking out Fos reduces seizure-induced plasticity (Watanabe et al., 1996), other signaling cascades such as mTOR (Kim et al., 2022), BDNF (Ramnauth et al., 2022) and the immediate early gene *Arc* (Larsen et al., 2005) can all be triggered by ECS-induced seizures. One way to explore the contribution of these plasticity pathways to treatment effects will be to map the gene expression changes following ECT more broadly.

Does ECT drive CSD in humans?

In addition to the results presented in this paper and that of (Rosenthal et al., 2025), there are three additional lines of evidence that support the hypothesis that ECT triggers CSD in patients:

1. A significant proportion of ECT patients suffer from a migraine-like headache immediately after the treatment (Mulder and Grootens, 2020). Migraines are thought to be caused by a CSD driven calcium influx that activates Panx1 channels (Karatas et al., 2013).
2. Confusion and cognitive side effects, with a particular focus on memory and hippocampus-dependent processes, are frequently reported following ECT (Impastato and Almansi, 1942; Porter et al., 2020). In mouse models of epilepsy, postictal confusion has been shown to be driven by hippocampal CSD, rather than by the seizure itself (Mitlasóczki et al., 2025).
3. CSD causes osmotic changes (Mazel et al., 2002) that could explain the structural imaging changes observed after a single ECT session (Takamiya et al., 2025; Verdijk et al., 2026), which are particularly pronounced in the hippocampus (Bracht et al., 2026; Wilkinson et al., 2017).

Our data show that metrics which predict a positive ECT treatment outcome also correlate with the occurrence of CSD (Figure 6). Given that standard ECT protocols optimize for these metrics as a proxy for seizure quality (Krystal et al., 1995; Sackeim et al., 1991), it is possible that clinical practice has inadvertently optimized ECT to trigger CSD. If CSD accounts for plasticity effects, triggering a CSD in a non-seizure context may be sufficient to elicit therapeutic effects. This is supported by the clinical success of ultra-brief stimulations treatments that do not cause seizures, such as rTMS with accelerated protocols, which achieves treatment efficacy on par with ECT for major depressive disorder (Cole et al., 2022). Similarly, ultrasound stimulation can

trigger CSD in mice (Estrada et al., 2021) and functions as a treatment for major depressive disorder (Oh et al., 2024). Much like using a landslide to create ripples in a pond, a generalized seizure may be an unnecessarily burdensome way to trigger the CSD required for treatment-relevant plasticity effects.

CSD as a driver of ECT related plasticity

The massive intracellular calcium influx during CSD (Figure 2, 4) is a prime candidate for driving the molecular changes underlying ECT-induced neuronal plasticity. Calcium is the entry point for a variety of plasticity-related signaling pathways that are disrupted in psychiatric conditions (Nanou and Catterall, 2018). While both physiological activity and seizures can trigger these pathways, CSD stands out due to the sheer magnitude of its calcium surge, driven in part by a near-total release of endoplasmic reticulum stores (Stern et al., 2024). Elevated calcium levels drive the expression of key plasticity markers. For instance, CSD-induced calcium triggers the Fos signaling cascade (Iqbal Chowdhury et al., 2003) and promotes the expression of BDNF (Faraguna et al., 2010). As the primary ligand for the TRKB receptor, BDNF activates a pathway that is a well-established target for both antidepressant (Casarotto et al., 2021) and antipsychotic drugs (Pandya et al., 2013).

While we cannot fully exclude the possibility of a secondary event, such as a unilateral seizure restricted to the CSD hemisphere, we monitored calcium activity in a subset of mice (11/17) until shortly before euthanasia and did not see any seizure-like calcium activity. We also did not observe behavioral signatures of a seizure in any of the mice. But even if secondary events did occur, the first unilateral event we observed was the CSD. This, combined with the fact that the CSD provides a potent biological mechanism to explain the robust neuroplasticity driven by ECT, leads us to conclude that the CSD is the primary treatment relevant event triggered by ECT, and not the phase III oscillation.

Origin of phase III oscillation

In the ECT literature, the phase III oscillation is often referred to as a seizure. We suspect that the key difference to an epileptic seizure is that an initial strong input (either directly from the ECS or indirectly via ECS driven excitation of cortex) to thalamus triggers a 2-4 Hz oscillation (Bal et al., 2000). At the same time, ECS stochastically triggers CSDs. As these move across cortex they silence cortical activity, and what remains in their wake is the oscillatory drive from thalamus. A central thalamic is consistent with the observation that phase III oscillations have zero phase lag across the human cortex (Brumback and Staton, 1982; Huels et al., 2023). In response to ECS, this gives rise to a phase III oscillation that does not have the ictal spikes characteristic of epileptic seizures. Ictal spikes in epileptic seizures are thought to reflect cortical responses to the oscillating thalamic drive (Meeren et al., 2002; Polack et al., 2009). Interestingly, a combination of CSD induced plasticity and the phase III oscillation (Figure 3D) could result in a selective strengthening of thalamocortical synapses. It has been speculated that such an increase is the mechanism that underlies the therapeutic efficacy of ECT (Wei et al., 2020). Assuming psychosis is the result of thalamocortical coupling that is too weak in frontal areas of the cortex (Keller and Sterzer, 2024), this mechanism of action could explain both the efficacy of ECT in treating psychosis and why patients with psychotic depression have more favorable ECT treatment outcomes than those with nonpsychotic depression (Petrides et al., 2001).

Future directions

Unresolved is the question of how to reconcile the non-specific nature of CSD with the cell type specific effects that characterize rTMS (Gongwer et al., 2025), antidepressant (Shao et al., 2025; Vesuna et al., 2020) and antipsychotic drugs (Heindorf and Keller, 2024; Lupori et al., 2026). Several lines of evidence suggest that the effects of CSD may also be cell type specific. First, CSD is easier to trigger in superficial than in deeper layers of cortex (Leo and Morison, 1945), and affects superficial somata for a significantly longer duration (Figure 4). This aligns with the evidence that schizophrenia is associated to a number of plasticity-related genes whose

expression is selectively enriched in upper cortical layers (Batiuk et al., 2022). Second, the large spectrum of time courses of calcium responses to CSD (Figure 4) could be explained by cell type intrinsic mechanisms, such as differential NMDA receptor expression (Buchanan et al., 2012). Testing this hypothesis will require cell type specific chronic calcium imaging following ECS.

The immediate clinical challenge stemming from our findings will be to determine whether the role of CSD is therapeutically beneficial or potentially deleterious. Optimizing ECT involves balancing the likelihood of positive therapeutic outcomes while minimizing adverse cognitive effects, most notably retrograde amnesia and impairments in autobiographic memory (Porter et al., 2020; Sackeim et al., 2007). For example, there is an optimal window for the stimulation charge: while a minimum stimulation charge is required for therapeutic benefit, a stimulation charge significantly exceeding the phase III oscillation threshold is linked to increased cognitive side effects (Delva et al., 2000; Sackeim et al., 1987). This could be explained if a higher stimulation charge is more likely to trigger CSDs in brain regions more distant from the stimulation electrodes. For example, it is conceivable that a CSD in frontal cortex is therapeutically beneficial while a CSD in hippocampus is responsible for retrograde amnesia. In mice, the ECS driven CSD likely invades hippocampus (Figure 5) (Mitlasóczki et al., 2025). If so, this might open up potential for pharmacological interventions to prevent a CSD invasion of hippocampus during ECT, e.g. with NMDA receptor antagonists that preferentially affect hippocampus (Mutel et al., 1998). By restricting CSD to the neocortex, it may be possible to prevent retrograde amnesia without compromising the cortical plasticity effects required for therapeutic outcomes.

Relevance

Our findings suggest that CSD, a currently unmonitored neuronal response to ECS, appears to be the primary driver of ECT-induced neuroplasticity. Ultimately, we propose that monitoring and facilitating CSD during ECT may unlock the possibility to transform psychiatry's most potent intervention into a targeted and reliable therapy with minimal side effects.

Methods

Mice

A total of 66 mice (27 male, 39 female), 7 – 22 weeks old at the start of the experiment, were used. Most mice were C57BL/6, but for two-photon prism imaging, the cohort also included PlexinD1-CreERT2 heterozygous mice. In the PlexinD1-CreERT2 mice, tamoxifen food was administered to induce ChrimsonR expression in the retrosplenial cortex for a separate experiment. See Table S2 for details of mouse inclusion for the different experiments. Mice were group-housed in a vivarium (light/dark cycle: 12/12 hours), and experiments carried out in light cycle. In female mice, we did not time experiments to a specific phase of the estrous cycle. All animal procedures were approved by and carried out in accordance with the guidelines of the Veterinary Department of the Canton of Basel-Stadt, Switzerland.

Surgery

For all surgical procedures, mice were anesthetized with a mixture of fentanyl (0.05 mg/kg; Actavis), midazolam (5.0 mg/kg; Dormicum, Roche), and medetomidine (0.5 mg/kg; Domitor, Orion) injected intraperitoneally. Analgesics were applied perioperatively (2% lidocaine gel, meloxicam 5 mg/kg) and postoperatively (3.25 mg/kg; Ethiqa XR). Eyes were covered with ophthalmic gel (Virbac Schweiz AG). For widefield imaging, we implanted crystal skull (Kim et al., 2016) or thinned skull (Yang et al., 2010) cranial windows. Briefly, the perimeter of the skull plate overlying the cortex was thinned using a dental drill until it could be removed with forceps (crystal skull) or only thinned in its entirety until transparent but not removed (thinned skull). To protect the brain, a glass or acrylic polymer window was then implanted. For two-photon imaging, a cranial window was implanted over primary visual cortex (V1) as previously described (Keller et al., 2012; Leinweber et al., 2014). Briefly, a 4 mm craniotomy was made over the right V1, centered 2.5 mm lateral and 0.5 mm anterior to lambda. The exposed cortex was sealed with a 3

mm or 4 mm circular glass coverslip. For prism imaging, a 0.7 mm glass prism (Tower Optical Corporation) was attached to the coverslip with UV-curable glue (Norland Optical Adhesive), and a small incision of cortical tissue was made to allow for the insertion of the prism into the cortex. Cranial windows were sealed using gel superglue (Ultra Gel, Pattex), and, for widefield windows, cyanoacrylate adhesive (Vetbond, 3M) (Kauvar et al., 2020). The remaining exposed surface of the skull was covered with cyanoacrylate adhesive, and a titanium head bar was fixed to the skull using dental cement (Paladur, Heraeus Kulzer). After surgery, anesthesia was antagonized by a mixture of flumazenil (0.5 mg/kg; Anexate, Roche) and atipamezole (2.5 mg/kg; Antisedan, Orion Pharma) injected intraperitoneally.

Virus injections

For widefield experiments, we deposited an AAV vector with PHP.eB capsid (Chan et al., 2017) retro-orbitally (4 µl per eye of at least 10^{14} GC/ml) to drive expression throughout cortex of GCaMP6s (AAV-PHP.eB-Ef1α-GCaMP6s-WPRE) or EGFP (AAV-PHP.eB-Ef1α-EGFP-WPRE). For two-photon experiments, the AAV was injected locally to drive expression of GCaMP6f (AAV2/9-Ef1α-GCaMP6f-WPRE). Imaging commenced at the earliest 3 weeks after AAV injection.

Electroconvulsive stimulation (ECS) in mice

For all ECS experiments mice were anesthetized with isoflurane (2%) using 95% O_2 as a gas carrier (1 L/min). For myorelaxation we injected succinylcholine chloride (1 mg/kg; Sigma-Aldrich) intraperitoneally. Mice were head-fixed, and ECS was delivered through auricular electrodes (Ugo Basile model #57802) using a pulse generator (Ugo Basile model #57800-001). A conductive salt-free electrolyte gel (Spectra 360 gel, Parker Laboratories) was applied to the electrodes to improve conductivity. Stimulation consisted of a 1 s long pulse train with a frequency of between 25 and 100 Hz, and a current amplitude of between 15 and 75 mA. Pulse width was 0.5 ms, which resulted in a total charge range of between 0.187 and 3.750 mC. These parameters reliably evoke tonic-clonic convulsions in mice (Hagen et al., 2015; van Buel et al., 2017). For comparison, patient ECT parameters used here were typically as follows: train duration up to 8 seconds, pulse width 0.5-1 ms, a fixed current amplitude of 900 mA, pulse frequency between 40-60 Hz, charge maximum 1000 mC. Thus, stimulus duration, current amplitude and resulting total charge are adapted to the mouse, but frequency/pulse-width are within clinical range (Peterchev et al., 2010). Of note, the stimulation polarity was constant for mice ECS, whereas bidirectional pulse train (alternating polarity) was used for patient ECT. For sham ECS experiments, we used an identical procedure with no current delivery. Up to 6 ECS sessions were administered at intervals of 48 hours. Stimulation intensities and pulse characteristics were randomized across subjects to eliminate order effects.

Electroconvulsive therapy (ECT) in humans

The retrospective treatment data of 28 random patients (10 male, 18 female, all > 18 years old), who underwent ECT at the Zentrum für Affektive, Stress-und Schlafstörungen (ZASS), University Psychiatric Clinics (UPK), Basel due to a psychiatric indication were included. Patients signed a general consent form (approved by the local ethics committee). All patient procedures were approved by and carried out in accordance with the Ethikkommission Nordwest-und Zentralschweiz (EKNZ). One randomly chosen treatment within the first half of the ECT acute treatment series (i.e. < 7^{th} treatment) per person was considered for analysis. Restimulation treatment data were excluded. Medical indication for ECT, patient information, treatment preparation and anesthesia followed standardized clinical protocols according to current standards of care. ECT was conducted with bifrontal stimulation using the Thymatron® System IV device (Somatics, LLC. Lake Bluff, IL, USA) and disposable adherent stimulus electrodes (EPAD, Thymapad®), as previously described (*The Practice of Electroconvulsive Therapy Third Edition*, 2025), following Kellner's ECT guidelines (Kellner, 2018). Briefly, patients were anesthetized with either propofol or etomidate (Braun Medical AG) and myorelaxed with succinylcholine chloride (Amino AG). Skin surface was cleansed using an alcohol-containing solvent and abrasive gel. A

conductive and adhesive liquid (Signaspray®, Parker Laboratories) was then applied to the skin. EEG was recorded at 200 Hz using bilateral frontomastoid placement and filtered using a band-pass with 3dB points at 2 and 25 Hz. We excluded the first two seconds of recording following the stimulation to remove a capacitive coupling artifact. ECT was performed about 4 min after the injection of etomidate and 5 min after the injection of propofol, using the 'double dose' stimulation protocol. ECT sessions included in the analysis were performed by multiple clinicians with standardized preparation and stimulation procedures. Data were measured using the Thymatron during each session, including stimulation parameters and EEG derived seizure quality parameters. In addition, we had access to formalized clinical documentation listing the administered medication and manually assessed seizure duration. Digitalization of stored ECT data for the current analysis was performed after December 2020 using GENET-GPD (Freundlieb et al., 2023). The digitalized treatment data were derived from the GENET-GPD database. Patient data were stored in the UPK patient case files in compliance with accepted data protection and record-keeping regulations.

Electroencephalography (EEG) in mice

Mice were anesthetized as described above, and the glass or polymer window was removed. An EEG multielectrode array with 30 recording sites (EEG mouse-30-A-10-H32, Neuronexus) was used to record neural activity across the surface of the dorsal cortex. Signals were amplified using a 32 channel headstage (RHD 32ch, Intan Technologies) and digitized at 30 kHz using an Open Ephys acquisition board (Siegle et al., 2017). During ECS delivery, the EEG array was physically disconnected by an electronically triggered relay to prevent electrical arcing between electrodes. EEG data was downsampled to 1 kHz and band-pass filtered between 0.5 and 10 Hz. We excluded the first two seconds of recording following EEG reconnection to remove a capacitive coupling artifact (Figure S1). As the concurrent widefield calcium signal provided an unambiguous polarity reference, the polarity of the EEG signal is such that positive voltage deflections corresponded to increases in fluorescence.

Widefield imaging

Widefield imaging experiments were conducted on a custom-built macroscope with objectives mounted face-to-face (Nikon 85 mm/f1.8 sample side, Nikon 50 mm/f1.4 sensor side). A 470 nm LED (Thorlabs) powered by a custom-built LED driver was used to excite fluorescent indicators through an excitation filter (SP490, Thorlabs) reflected off of a dichroic mirror (LP490, Thorlabs) placed parfocal to the objectives. The fluorescence was collected through a 525/50 emission filter on a sCMOS camera (PCO edge 4.2). LED illumination was adjusted with a collimator (Thorlabs SM2F32-A) to homogenously illuminate cortical surface through the cranial window. Images were acquired at 100 Hz frame rate. Raw images were cropped on the sensor and data was stored to disk with custom-written LabVIEW (National Instruments) software, resulting in an effective pixel size of 60 μm^2 at a resolution of 1108 by 1220 pixel (1.35 MP).

Two-photon imaging

Two-photon calcium imaging was performed using custom-built microscopes (Leinweber et al. 2014). The illumination source was a tunable femtosecond laser (Insight, Spectra Physics or Chameleon, Coherent) tuned to 930 nm. Emission light was band-pass filtered using a 525/50 filter and detected using a GaAsP photomultiplier (H7422, Hamamatsu). Photomultiplier signals were amplified (DHPCA-100, Femto), digitized (NI5772, National Instruments) at 800 MHz, and band-pass filtered at 80 MHz using a digital Fourier-transform filter implemented in custom-written software on an FPGA (NI5772, National Instruments). The scanning system of the microscopes was based on a 12 kHz resonant scanner (Cambridge Technology). Images were acquired at a resolution of 750 by 400 pixels (60 Hz frame rate) with a 16x, 0.8 NA water immersion objective (Nikon). We imaged layer 2/3 at a depth of 100-250 µm with a field of view of 375 by 300 µm. For prism imaging, to enable imaging of as much cortical depth as possible, the field of view was

expanded to 270 by 960 μm, at a resolution of 750 by 800 pixels. This resulted in an effective frame rate of 30 Hz. Laminar boundaries were estimated from the density of GCaMP6-expressing cells, which typically peaks in layer 2/3 and upper layer 5 (Andermann et al., 2013).

Image processing

For analysis of chronic widefield macroscope imaging, raw movie data was manually registered across days by aligning subsequent mean projections of the data to the first recorded image sequence. In the raw 1108 by 1220 pixel images, we tiled the cortex with 818 ROIs each with a fixed location relative to bregma and lambda. This resulted in an average ROI size of 25 by 25 pixels (approximately 230 by 230 μm). Each ROI was also registered against the Allen Institute Mouse Brain Coordinate Framework (Wang et al., 2020). In concurrent EEG and widefield recordings, we defined annular ROIs centered on each of the 30 electrode sites. The inner boundary corresponded to the electrode footprint with a 50 μm buffer (approximately 60 pixels in diameter; approximately 550 μm) and was excluded from analysis, while the outer boundary defined a circular region with a diameter of approximately 80 pixels. Two-photon calcium imaging data were processed as previously described (Attinger et al., 2017; Keller et al., 2012). Briefly, raw images were full-frame registered to correct for lateral brain motion. Somata ROIs were manually selected based on mean and maximum fluorescence images. For each somata ROI, a corresponding neuropil ROI of equal pixel area was created as a surrounding annulus, maintaining a 3-pixel exclusion buffer and avoiding overlap with other defined ROIs. No neuropil subtraction to somata activity was done. Activity was calculated as the $\Delta F/F_0$, where F_0 was the median fluorescence of the recording before ECS (typically 30 seconds). ECS recordings lasted for 5 min.

Histology

Mice underwent a single ECS or sham procedure while being monitored for calcium events through widefield imaging and were returned to their home cage for one hour. A subset (11/17) of mice was instead kept head-fixed and imaged for 1 hour to verify that no additional calcium events occurred. Mice were then anesthetized with a mixture of fentanyl (0.05 mg/kg; Actavis), midazolam (5.0 mg/kg; Dormicum, Roche), and medetomidine (0.5 mg/kg; Domitor, Orion), and transcardially perfused with phosphate-buffered saline (PBS) solution and subsequently with ice-cold 4% paraformaldehyde (PFA) in PBS. Brains were extracted and post-fixed overnight in 4% PFA at 4 °C. They were then embedded in 4% agarose and coronally sectioned through the entire anteroposterior extent of the cortex at (50 μm thickness) using a vibratome (Leica VT100S). We collected every fourth section for further processing, resulting in an effective sampling step of 200 μm. Free-floating sections were then processed for Fos immunohistochemistry. Briefly, sections were blocked for 2 h at room temperature in a solution containing 5% donkey serum (BSA, Sigma-Aldrich) and 0.5% Triton X-100 in PBS, then incubated overnight at 4 °C with a solution containing anti-Fos antibody (226008, Synaptic Systems, 1:1000), 1% Donkey Serum and 0.1% Triton X-100 in PBS. Wells were then rinsed 3 times in PBS (10 min each) and incubated with a solution containing donkey polyclonal anti-rabbit antibody (A31573, Invitrogen, Alexa Fluor™ 647 conjugate, 1:300), 1% Donkey Serum and 0.1% Triton X-100 in PBS for 2 h at room temperature. Following additional 10-minutes PBS washes, nuclei were counterstained with DAPI (Sigma-Aldrich, 1:1000) for 10 minutes. Finally, sections were mounted on microscopy slides with a mounting medium (VECTASHIELD, H-100, Vector Laboratories), sealed with nail polish, and stored at 4°C. Images were then acquired with an Axioscan Z1 (Zeiss) microscope using an apochromatic 10x/0.5 M27 objective (Zeiss). Fluorophores were excited with 422 nm and 668 nm X-Cite Xylis LED. The emission wavelength were filtered with a BP 445/50 filter for DAPI and a BP690/50 filter for Alexa 647. Images were collected with an Hamamatsu ORCA flash 4.0V camera at a pixel size of 0.650 μm.

Tissue registration and quantification

Images were aligned to the Allen Mouse Brain Common Coordinate Framework (CCFv3-2017) as described previously (Lupori et al., 2023). All preprocessing and registration steps, unless stated otherwise, were carried out using custom-written MATLAB (MathWorks) code. For each brain, images were ordered along the posterior-to-anterior direction. Based on a reference mark identifying the right side and/or tissue irregularities, images were mirrored vertically so that all matching hemispheres would be on the same side. Binary masks to restrict quantification to brain tissue were automatically generated from the DAPI images by training a pixel classifier in Ilastik (Berg et al. 2019). Each mask was then visually inspected and manually adjusted based on the Fos images, to remove regions containing tissue damage or staining artifacts. Left-right binary masks defining which hemisphere a pixel belongs to were then generated by manually drawing a segment at the midline of each slice. Using the DAPI images, each slice was matched to a plane in the CCFv3 though one first step of global alignment using QuickNII v2.2 (Puchades et al. 2019) and a second step of local non-rigid transformation with VisuAlign v0.9 (*RRID:SCR_017978*, VisuAlign). For cell counting, Fos channel images were first pre-processed with a rolling ball filter (50 pixels or 32.5 μm radius) for background removal. Cell detection and counting were then performed on the filtered images with custom scripting inside QuPath v.0.6.0 (Bankhead et al. 2017). Briefly, we used the inbuilt automatic cell detection tool to identify Fos-positive cells using the median fluorescence of the slide as a threshold. A random forest classifier was then trained to remove detection artifacts. For each cell, we calculated mean pixel intensity and x-y coordinates of the centroid. For all regions descending from isocortex, as per the hierarchy defined in the CCFv3, we computed cell density (number of cells/total area in mm2), mean cell intensity, and energy (cell density*mean cell intensity) (Lein et al., 2007; Lupori et al., 2023). For each metric, the value was then normalized by the average of that metric across all sham-treated mice.

Data analysis

All data analysis was performed with custom-written MATLAB (MathWorks) code.

When visualizing data with a box plot, the central box indicates the interquartile range (IQR), spanning from the first (Q_1) to the third (Q_3) quartiles. Whiskers extend to data points not considered outliers. Outliers were defined as data points lying outside of the Q_1 – 1.5 IQR to Q_3 + 1.5 IQR range. A central horizontal line indicates the median and an open circle the mean of the distribution. To represent the underlying probability density, a Kernel Density Estimate was computed using a Parzen-window method with a normally distributed kernel.

In Figure 1 and Figure 6, spectrograms were computed using a 2 s sliding window with 95 % overlap of the band-passed signal between 0.5 and 10 Hz. Power spectral density was estimated for each channel or ROI independently and converted to decibel scale. Oscillations were detected in the 1-5 Hz band by computing the Hilbert envelope of the EEG signal. Oscillation onsets were defined as the first crossing of the 90^{th} percentile of the envelope after ECS. Oscillation terminations were defined as the first time the envelope dropped below a baseline threshold. Patient EEG is interrupted rapidly after the termination of oscillations. To account for the differences in recording length, the termination threshold was set as the 50^{th} percentile Hilbert envelope for mice and as the 5^{th} percentile for patients. For patient EEG, this detection method yielded oscillation durations not statistically different to those computed by the proprietary Thymatron algorithm (hierarchical bootstrap with resampling, $p = 0.268$). Power-weighted mean frequencies were computed as the sum of power values in a frequency, multiplied by that frequency. We reported the median values in a 2 s window centered on the global frequency peak and in the final 2 s of the detected oscillation. For mouse widefield data, the onsets and offsets time were computed from the concurrent EEG signal. We excluded frequencies between 7 and 9 Hz, if they exceeded 90 μV; these regions were dilated by 2 s and masked-out from further analysis. We completely excluded EEG electrodes and their associated widefield ROI if the onset/offset values were non-finite or if the total duration of oscillation was less than 1s, resulting in the exclusion of 78/480 (16%) of electrodes in our dataset.

In Figure 2, and Figure S3, calcium event speed was estimated through the local fluorescence gradient. Peak latencies were defined as the global maximum occurring 10 to 200 seconds after local wavefront onset. For each ROI, raw fluorescence values were low-passed filtered below 0.5 Hz and a plane ($t = S_x x + S_y y + t_0$) was fitted to the peak latencies of neighbors within a 0.8 mm radius using bisquare weighting. This determined a local slowness vector, the magnitude of which was inverted to determine speed. Speed values deviating more than 3.5 median absolute deviation from the session median were excluded. For two-photon imaging, propagation speed was calculated as the median velocity of calcium events across pairs of somata ROIs separated by at least 200 µm.

In Figure 2, and Figure S4, the period of direct ECS stimulation is defined as the first 5 s post ECS onset, based on the duration reported in Figure S1.

In Figure 2, 3, and Figure S3, the onset of a calcium event was defined as the first crossing of 150% the mean calcium activity before ECS. Only events occurring 10 s after ECS were considered as calcium events. For analysis of time to peak, we excluded ROIs for which there was no clear separation between direct ECS response and calcium event. To determine the presence of an oscillation, we averaged the calcium traces across hemispheres and used the same algorithm used in Figure 1 and Figure 6. To characterize the probability of calcium event or oscillation as a function of ECS parameters, we fitted a linear slope with ordinary least squares method. 95% confidence bands for the mean predicted response were computed across the range of predictor variables.

In Figure 2, to generate isochrones, we set a ROI-wise threshold to 150% of the maximum ECS baseline activity. The first time at which each ROI crossed this threshold was used to construct a time-of-activation map, which was then filtered with a normal distribution. Contour lines were extracted at 2 second intervals from the onset of calcium event until 50 s post-onset.

In Figure 4, cortical layers were separated in supragranular and infragranular, based on empirical distribution of cell densities, which shows a clear gap in cortical layer 4. To compare the activity of somata with their neuropil, we aligned each somata with the peak of its neuropil during calcium events. This alignment ensures that the propagation delay across the field of view is not taken into account. To compare supragranular and infragranular layers, somata were instead aligned to the max of a neuropil trace, averaged across all neuropil ROIs in the entire recording. To quantify the dynamics of GCaMP6f fluorescence following the calcium event, we computed a linear recovery slope with least-square ordinary fit in the 2 to 60s seconds following peak somata signal.

In Figure 6, the mid-ictal amplitude was computed as the mean of all oscillation peaks in a 4 s window centered at the duration of the oscillation (Krystal et al., 1995). The postictal suppression index was defined as the ratio of the median 1-30 Hz envelope amplitude post-oscillation over intra-oscillations. Welch's periodogram method was used to compute the inter-hemispheric coherence between pairs of symmetric electrodes. We reported the values of coherence in the 1 to 5 Hz band.

In Figure S2, to illustrate the synchronicity of EEG and calcium signals, oscillation peaks in the EEG channel were detected using the Automatic Multiscale Peak Detection algorithm, which is suited to non-stationary signals, such as EEG, without requiring manual parameter tuning or pre-filtering (Scholkmann et al., 2012).

Statistical analysis

All statistical information for the tests performed in the manuscript is provided in Table S1. Analyses accounted for the nested structure of the data consisting of recording units (neurons, EEG channels or ROIs) within subjects (mice or patients) using hierarchical bootstrap (Saravanan et al., 2020). Briefly, we first resampled with replacement data at the subject level and then resampled with replacement a second time at the recording unit level. We then computed the mean of this bootstrap sample and repeated this N times to generate a bootstrap distribution of the mean estimate. For all statistical testing the number of bootstrap samples (N) was 10 000, for

plotting bootstrap mean and standard error response curves it was 1000. The bootstrap standard error is the 68% confidence interval (1 SD, 15.8th percentile to 84.2nd percentile) in the bootstrap distribution of the mean.

To account for the false discovery rate in multiple comparisons, we applied an adjustment to p-values (Benjamini and Hochberg, 1995). Briefly, p-values were sorted in ascending order and multiplied by the ratio of the total number of comparisons within a data group (for example, all bootstrap tests for a specific EEG metric) to their sorting rank. The final significance cutoff was determined by finding the largest p-value smaller than its rank-specific threshold, at which point all p-values with a higher rank (i.e., those with smaller p-values) were also rejected.

For linear regression analysis, we computed the F-statistic to test the significance of the model. This test evaluates whether the slope is significantly different from zero by comparing the model degrees of freedom (the number of predictors, here, one) against the degrees of freedom for error (the number of observations minus the parameters for the intercept and slope). The resulting F-statistic represents the ratio of explained variance to unexplained variance, quantifying the portion of the data's variability accounted for by the linear regression. For multivariate linear regression analysis, we measured the probability of occurrence of a calcium event as a function of stimulation amplitude, frequency, and their two-way interaction. For each of those three parameters, we performed a two-sided t-test against the null hypothesis that this parameter is equal to zero.

Data availability

Software for controlling the two-photon and widefield microscopes and preprocessing of calcium imaging data is available on *https://sourceforge.net/projects/iris-scanning/*. All mouse data and code necessary to generate the figures of this manuscript will be deposited upon acceptance to zenodo.org. Patient data will be made available upon reasonable request.

Supplementary figures and tables

REAGENT OR RESOURCE	SOURCE	IDENTIFIER
Bacterial and virus strains		
AAV-PHP.eB-EF1α-GCaMP6s-WPRE (10^{14} GC/ml)	FMI vector core	vector.fmi.ch
AAV-PHP.eB-EF1α-EGFP-WPRE (10^{14} GC/ml)	FMI vector core	vector.fmi.ch
AAV2/9-EF1α-GCaMP6f-WPRE (10^{14} GC/ml)	FMI vector core	vector.fmi.ch
AAV2/1-hSyn-DIO-ChrimsonR-tdTomato (10^{14} GC/ml)	FMI vector core	vector.fmi.ch
Chemicals, peptides, and recombinant proteins		
Fentanyl citrate	Actavis	CAS 990-73-8
Midazolam (Dormicum)	Roche	CAS 59467-96-8
Medetomidine (Domitor)	Orion Pharma	CAS 86347-14-0
Ropivacaine	Presenius Kabi	CAS 132112-35-7
Lidocaine	Bichsel	CAS 137-58-6
Buprenorphine hydrochloride (Ethiqa XR)	Fidelis Pharmaceuticals	CAS 53152-21-9
Ophthalmic gel (Humigel)	Virbac	N/A
Flumazenil (Anexate)	Roche	CAS 78755-81-4
Atipamezole (Antisedan)	Orion Pharma	CAS 104054-27-5
N-Butyl-2-cyanoacrylate (Vetbond)	3M	CAS 6606-65-1
Dental cement (Paladur)	Heraeus Kulzer	CAS 9066-86-8
Spectra 360 electrode gel	Parker Laboratories	N/A
Attane Isoflurane	Provet AG	CAS 26675-46-7
Succinyl choline chloride	Sigma-Aldrich	CAS 6101-15-1
Paraformaldehyde (PFA)	Sigma-Aldrich	CAS 30525-89-4
Agarose	Sigma-Aldrich	CAS 9012-36-6
Donkey Serum (BSA)	Sigma-Aldrich	CAS 9048-46-8
Triton X-100	Sigma-Aldrich	CAS 9002-93-1
Primary anti-Fos antibody	Synaptic Systems	N/A
Secondary anti-rabbit antibody (Alexa Fluor TM 647 coupled)	Invitrogen	N/A
DAPI	Sigma-Aldrich	28718-90-3
Mounting Medium (VectaShield Antifade)	Vector Laboratories	N/A
Deposited data		
All mouse data and code used to generate manuscript figures	This paper	zenodo.org
Patient data	This paper	On request
Experimental models: Organisms/strains		
Mus musculus: C57BL/6	Charles River	N/A
Mus musculus: 129S4-Plxnd1tm1.1(cre/ERT2)Zjh/J	Jackson Laboratories	RRID:IMSR_JAX:036294
Software and algorithms		
MATLAB (2023b)	The MathWorks	RRID:SCR_001622
LabVIEW	National Instruments	RRID:SCR_014325
Python	python.org	RRID:SCR_008394

Key resources table.

Figure	Description	Test	N_1	N_2	Unit	p-value (p_{adj})
1G	Oscillation duration in mouse EEG (N_1) vs patient EEG (N_2)	Two-tailed hierarchical bootstrap	402 (16)	50 (26)	Electrodes (mice) vs electrodes (patients)	0.34
1H	Power-weighted mean frequency					
	Mouse WF peak (N_1) vs offset (N_2)	Two-tailed hierarchical bootstrap, FDR adjusted	402 (16)	402 (16)	ROIs (mice)	0.0014 (0.0032)
	Mouse EEG peak (N_1) vs offset (N_2)	Two-tailed hierarchical bootstrap, FDR adjusted	402 (16)	402 (16)	Electrodes (mice)	< 0.0010 (< 0.0010)
	Patient EEG peak (N_1) vs offset (N_2)	Two-tailed hierarchical bootstrap, FDR adjusted	50 (26)	50 (26)	Electrodes (patients)	< 0.0010 (< 0.0010)
	Mouse WF peak (N_1) vs mouse EEG peak (N_2)	Two-tailed hierarchical bootstrap, FDR adjusted	402 (16)	402 (16)	ROIs (mice) vs electrodes (mice)	0.025 (0.034)
	Mouse WF offset (N_1) vs mouse EEG offset (N_2)	Two-tailed hierarchical bootstrap, FDR adjusted	402 (16)	402 (16)	ROIs (mice) vs electrodes (mice)	0.0018 (0.0032)
	Mouse EEG peak (N_1) vs patient EEG peak (N_2)	Two-tailed hierarchical bootstrap, FDR adjusted	402 (16)	50 (26)	Electrodes (mice) vs electrodes (patients)	0.092 (0.11)
	Mouse EEG offset (N_1) vs patient EEG offset (N_2)	Two-tailed hierarchical bootstrap, FDR adjusted	402 (16)	50 (26)	Electrodes (mice) vs electrodes (patients)	0.29 (0.29)
2D	Maximum ΔF/F0 in dorsal cortex					
	Pre-ECS (N_1) vs direct ECS response (N_2)	Two-tailed hierarchical bootstrap, FDR adjusted	77 (28)	77 (28)	ECS (mice)	< 0.0010 (< 0.0010)
	Pre-ECS (N_1) vs calcium event (N_2)	Two-tailed hierarchical bootstrap, FDR adjusted	77 (28)	23 (19)	ECS (mice)	< 0.0010 (< 0.0010)
	Direct ECS response (N_1) vs calcium event (N_2)	Two-tailed hierarchical bootstrap, FDR adjusted	77 (28)	23 (19)	ECS (mice)	< 0.0010 (< 0.0010)
3F	Linear regression of ECS charge against probability of calcium event	F-test	1	14	Degrees of freedom vs Degrees of Freedom for Error	< 0.0010
3G	Linear regression of ECS charge against probability of oscillation	F-test	1	14	Degrees of freedom vs Degrees of Freedom for Error	0.049
4E	Mean ΔF/F0 during calcium event in superficial layers somata (N_1) vs deep layers somata (N_2)	Two-tailed bootstrap	236	134	ROIs	see Figure
4F	Time of 50% max. ΔF/F0 in superficial layers somata (N_1) vs deep layers somata (N_2)	Two-tailed hierarchical bootstrap	236 (3)	134 (3)	ROIs (mice)	< 0.0010
4H	Mean ΔF/F0 during calcium event in somata (N_1) vs neuropil (N_2)	Two-tailed bootstrap	858	858	ROIs	see Figure
4I	Slope ΔF/F0 of somata (N_1) vs neuropil (N_2)	Two-tailed hierarchical bootstrap	858 (6)	858 (6)	ROIs (mice)	< 0.0010
5C	Fos energy fold-change vs. Sham ECS					
	Sham (N_1) vs no calcium event (N_2)	Two-tailed hierarchical bootstrap, FDR adjusted	10 (5)	14 (10)	Hemispheres (mice)	0.58 (0.58)

Table S1. Statistics table.

All values are rounded to two significant figures. The tests used were two-tailed hierarchical bootstrap, two-tailed bootstrap, one-tailed bootstrap, F-test, and t-test. Benjamini-Hochberg correction was used for false discovery rate (FDR) adjustment in multiple comparisons, in which case the adjusted p-value p_{adj} is the one reported in the associated figure and text. Sample sizes were estimated based on previous experiments performed in mouse behavioral paradigms (Attinger et al., 2017; Heindorf et al., 2018).

	No calcium event (N_1) vs calcium event (N_2)	Two-tailed hierarchical bootstrap, FDR adjusted	14 (10)	10 (8)	Hemispheres (mice)	< 0.0010 (< 0.0010)
	Sham (N_1) vs calcium event (N_2)	Two-tailed hierarchical bootstrap, FDR adjusted	10 (5)	10 (8)	Hemispheres (mice)	< 0.0010 (< 0.0010)
6C	Mid-oscillation amplitude					
	Direct ECS response (N_1) vs contra. calcium event (N_2)	Two-tailed hierarchical bootstrap, FDR adjusted	93 (4)	52 (4)	Electrodes (mice)	0.34 (0.34)
	Direct ECS response (N_1) vs ipsi. calcium event (N_2)	Two-tailed hierarchical bootstrap, FDR adjusted	93 (4)	257 (12)	Electrodes (mice)	< 0.0010 (< 0.0010)
	Contra. calcium event (N_1) vs ipsi. calcium event (N_2)	Two-tailed hierarchical bootstrap, FDR adjusted	52 (4)	257 (12)	Electrodes (mice)	0.016 (0.025)
6D	Oscillation duration					
	Direct ECS response (N_1) vs contra. calcium event (N_2)	Two-tailed hierarchical bootstrap, FDR adjusted	93 (4)	52 (4)	Electrodes (mice)	0.33 (0.50)
	Direct ECS response (N_1) vs ipsi. calcium event (N_2)	Two-tailed hierarchical bootstrap, FDR adjusted	93 (4)	257 (12)	Electrodes (mice)	0.00040 (0.0012)
	Contra. calcium event (N_1) vs ipsi. calcium event (N_2)	Two-tailed hierarchical bootstrap, FDR adjusted	52 (4)	257 (12)	Electrodes (mice)	0.52 (0.52)
6E	Postictal suppression index					
	Direct ECS response (N_1) vs contra. calcium event (N_2)	Two-tailed hierarchical bootstrap, FDR adjusted	93 (4)	52 (4)	Electrodes (mice)	0.13 (0.19)
	Direct ECS response (N_1) vs ipsi. calcium event (N_2)	Two-tailed hierarchical bootstrap, FDR adjusted	93 (4)	257 (12)	Electrodes (mice)	< 0.0010 (< 0.0010)
	Contra. calcium event (N_1) vs ipsi. calcium event (N_2)	Two-tailed hierarchical bootstrap, FDR adjusted	52 (4)	257 (12)	Electrodes (mice)	0.86 (0.86)
6F	Inter-hemispheric coherence					
	Direct ECS response (N_1) vs contra. calcium event (N_2)	Two-tailed hierarchical bootstrap, FDR adjusted	93 (4)	52 (4)	Electrodes (mice)	0.27 (0.61)
	Direct ECS response (N_1) vs ipsi. calcium event (N_2)	Two-tailed hierarchical bootstrap, FDR adjusted	93 (4)	257 (12)	Electrodes (mice)	0.41 (0.61)
	Contra. calcium event (N_1) vs ipsi. calcium event (N_2)	Two-tailed hierarchical bootstrap, FDR adjusted	52 (4)	257 (12)	Electrodes (mice)	0.70 (0.70)
S1B	Mean ΔF/F0 during ECS vs baseline	Two-tailed bootstrap	33105	-	ROIs	see Figure
S3A	Linear regression of ECS parameter against probability of calcium event					
	ECS frequency against probability of calcium event	F-test	1	2	Degrees of freedom vs Degrees of Freedom for Error	0.13
	ECS current against probability of calcium event	F-test	1	2	Degrees of freedom vs Degrees of Freedom for Error	0.052
	Multivariate linear regression of ECS parameter against probability of calcium event					
	ECS frequency against probability of calcium event	Two-sided t-test	1	12	Degrees of freedom vs Degrees of Freedom for Error	0.76

Table S1. (continued)

Table S1. (continued)

	ECS current against probability of calcium event	Two-sided t-test	1	12	Degrees of freedom vs Degrees of Freedom for Error	0.43
	Interaction of ECS frequency and ECS current against probability of calcium event	Two-sided t-test	1	12	Degrees of freedom vs Degrees of Freedom for Error	0.019
S3B	Linear regression of ECS parameter against probability of oscillation					
	ECS frequency against probability of oscillation	F-test	1	2	Degrees of freedom vs Degrees of Freedom for Error	0.37
	ECS current against probability of oscillation	F-test	1	2	Degrees of freedom vs Degrees of Freedom for Error	0.14
S4A	Linear regression of ECS charge against maximum ΔF/F0 during direct ECS response	F-test	1	2	Degrees of freedom vs Degrees of Freedom for Error	< 0.0010
S4B	Maximum ΔF/F0 during direct ECS response in ipsilateral (N_1) over contralateral hemisphere (N_2)	Two-tailed hierarchical bootstrap	16 (13)	16 (13)	ECS (mice)	0.0086
S5A	Mean ΔF/F0 during ECS					
	GFP (N_1) vs baseline	Two-tailed bootstrap	14190	-	ROIs	see Figure
	GFP (N_1) vs GCaMP6s (N_2)	Two-tailed bootstrap	14190	33105	ROIs	see Figure
S5C	Maximum ΔF/F0 in dorsal cortex during calcium event (N_1) vs EGFP event (N_2)	Two-tailed hierarchical bootstrap	23 (19)	8 (6)	ECS (mice)	< 0.0010
S5D	Propagation speed of calcium event (N_1) vs EGFP event (N_2)	Two-tailed hierarchical bootstrap	23 (19)	8 (6)	ECS (mice)	0.1084

Table S2. Number of subjects in each analysis.

Nbr. of subjects	Genotype	Experiment	AAV vector	Figures
16	C57BL/6	Concurrent widefield and EEG recordings	PHP.eB-Ef1α-GCaMP6s-WPRE	1, 5, S1, S2
28	-	Patient EEG	-	1
18	C57BL/6	Widefield calcium imaging without EEG	PHP.eB-Ef1α-GCaMP6s-WPRE	2, 3, S1, S3, S4, S5
17	C57BL/6	Widefield calcium imaging without EEG followed by Fos histology	PHP.eB-Ef1α-GCaMP6s-WPRE	2, 3, 6, S1, S3, S4, S5
8	C57BL/6	Widefield EGFP imaging	PHP.eB-Ef1α-EGFP-WPRE	S5
4	C57BL/6	Two-photon calcium imaging	2/9-Ef1α-GCaMP6f-WPRE	4
3	PlexinD1-CreERT2	Two-photon calcium imaging with microprism implant	2/9-Ef1α-GCaMP6f-WPRE 2/9-DIO-ChrimsonR-tdTomato	4

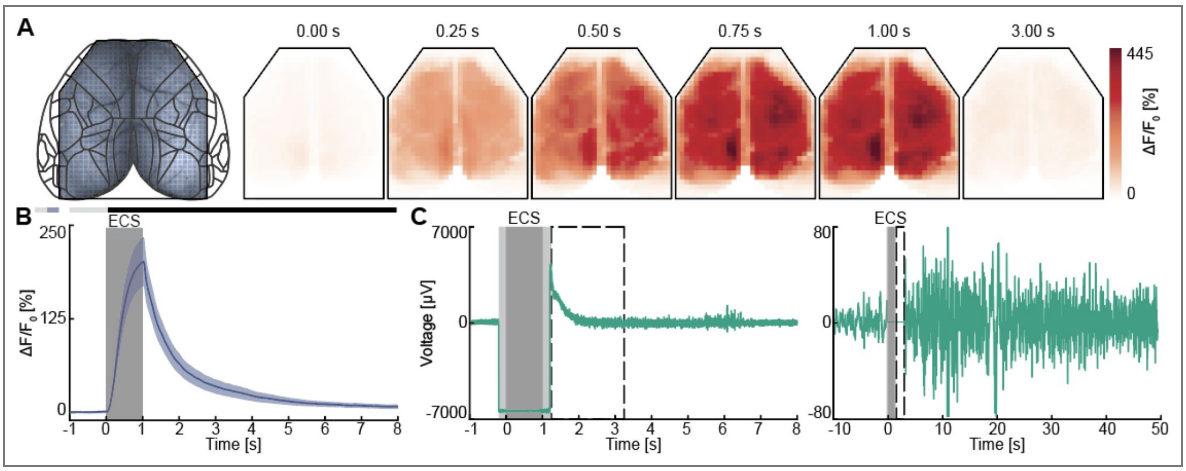

Figure S1. ECS triggers a direct calcium response during the EEG disconnection. Related to Figure 1.

(A) Left: Widefield recordings (without concurrent EEG) were parcellated into 818 ROIs, each of which was assigned to a cortical region according to the Allen Brain Atlas taxonomy. Right: Direct ECS calcium activity triggered by an example ECS. Each panel shows the average calcium activity over a 10 ms window starting at the time indicated above the panel. (B)Direct ECS calcium response estimated using hierarchical bootstrap across all ECS. Response curves are compared against baseline distribution for each time bin: in the horizontal bars above the plot, black marks time bins where $p<0.05$ and gray mark time bins where $p>0.05$. Duration of ECS is marked as a dark gray shaded area. (C)Left: during ECS (dark gray shaded area), the EEG electrode is temporarily disconnected to prevent arcing (Methods), leading to a period in which no EEG data is recorded (light gray shaded area). To eliminate the capacitive discharge artifact upon reconnection, the first 2 s of data are excluded from analysis (dashed box). Right: same signal with a longer time scale, following artifact removal and 0.5–10 Hz band-pass filtering.

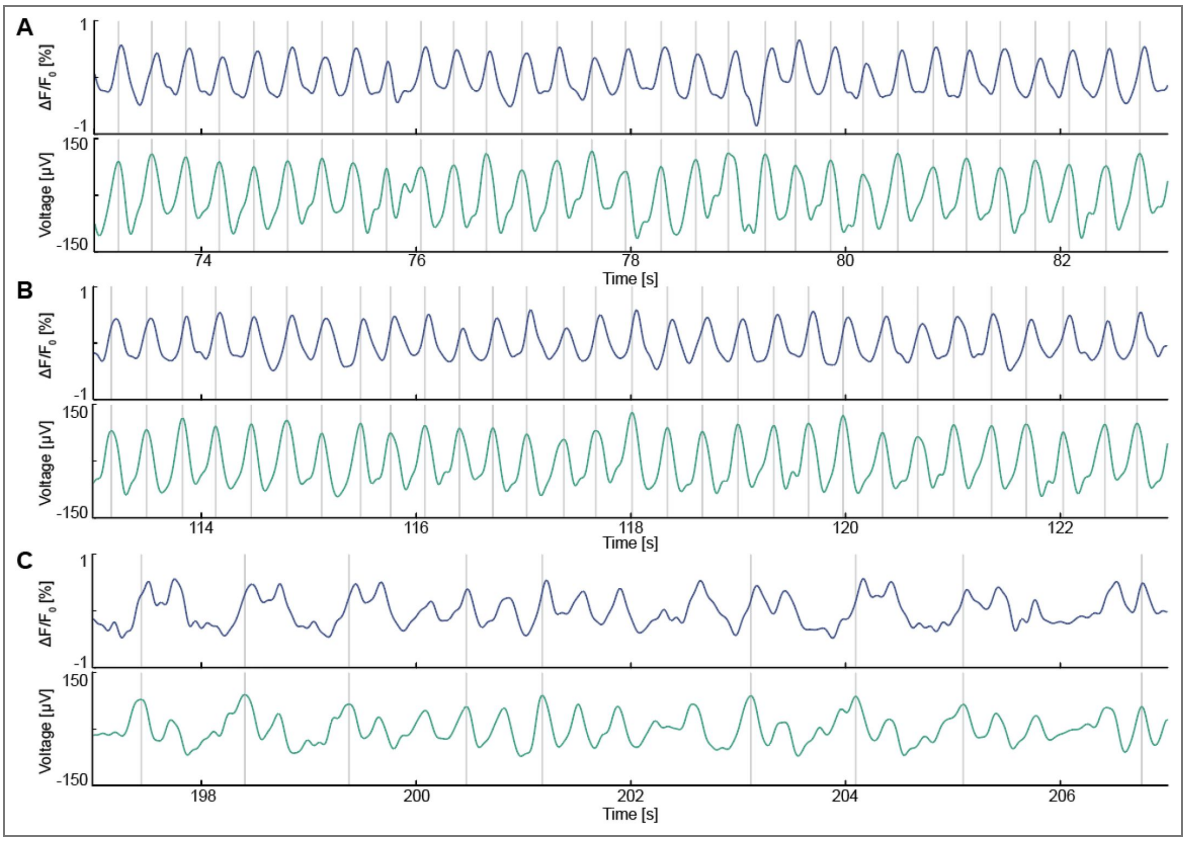

Figure S2. ECS triggered oscillations are synchronized between widefield calcium and EEG in mice. Related to Figure 1.

(A) Activity observed early after ECS in an example mouse widefield calcium imaging ROI (blue) and in the concurrently recorded EEG (green). Oscillations peaks were detected using Automatic Multi-scale Peak Detection on the EEG channel (Methods). (B)As in **A**, in a period of time 112 s after ECS. (C)As in **A**, in a period of time 197 s after ECS.

Figure S3. Influence of stimulation parameters on calcium events. Related to Figure 3.

(A) Probability of triggering a calcium event as a function of stimulation frequency (left) or current (right). The solid line represents the linear fit of the data; the shaded region represents 95% confidence interval on the fit. Error bars on individual data points indicate standard error. (B)As in **A**, but for oscillations. (C)Left: Distribution of calcium events speed across triplets of ROIs (see Methods). Right: Median calcium event speed as a function of stimulation charge. Dashed line indicates median calcium event speed across all charges. (D)Left: Distribution of the duration of calcium events in each widefield ROI (see Methods). Right: Median duration of calcium event as a function of stimulation charge. Dashed line indicates median duration across all charges. (E)Left: Delay from stimulation to calcium event onset. Right: Delay from stimulation to calcium event onset as a function of stimulation charge.

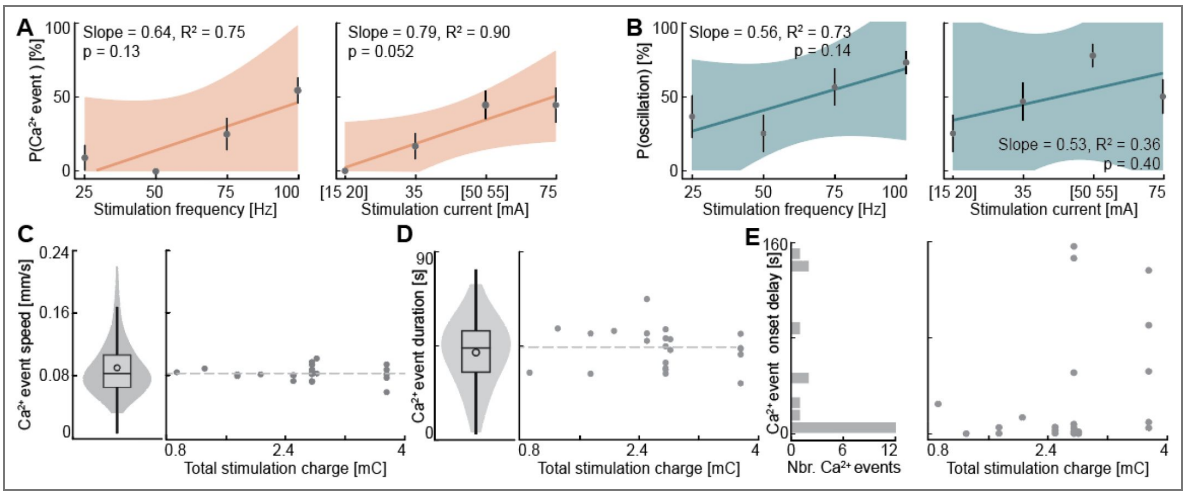

Figure S4. Direct ECS response in calcium imaging predicts the occurrence of calcium events. Related to Figure 3.

(A) Left: Maximum calcium activity during the direct ECS response as a function of stimulation charge. Red values are measured during ECS triggering a calcium event (either unilateral or bilateral) and gray values from ECS that did not trigger a calcium event. (B)Maximum calcium activity in both hemispheres fluorescence during the direct ECS response, before a unilateral calcium event was triggered.

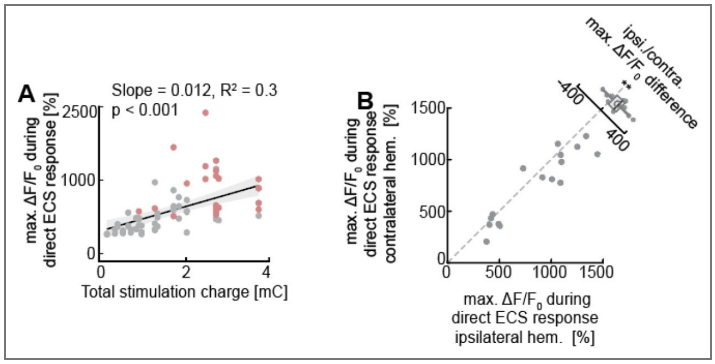

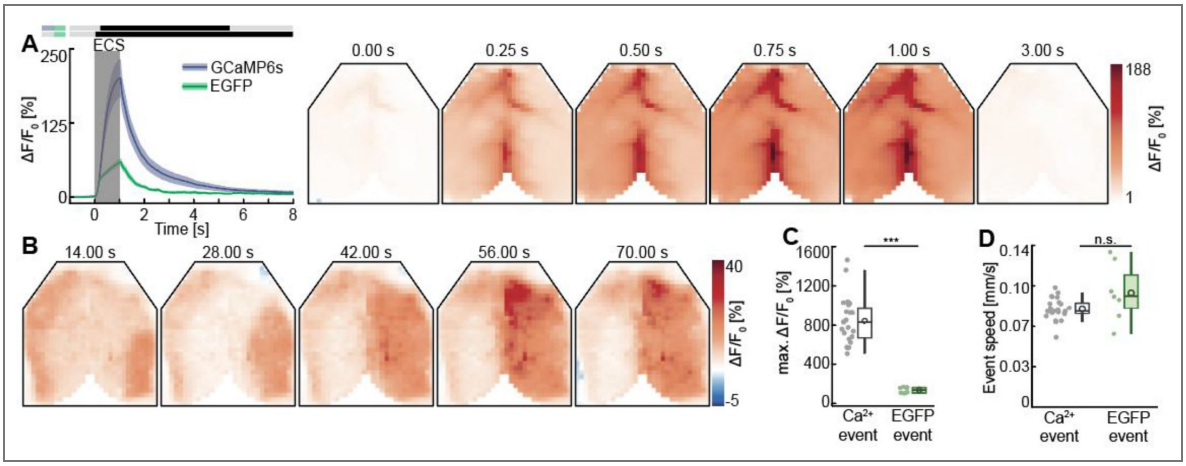

Figure S5. ECS triggers hemodynamic responses. Related to Figure 3.

(A) Left: Direct ECS fluorescence measured with GCaMP6s (as shown in Figure S1B) and EGFP, estimated across the population using hierarchical bootstrap. In the horizontal bars above the plot, black marks time bins where $p<0.05$ and gray mark time bins where $p>0.05$. The top bar represents the comparison between GCaMP6s and EGFP fluorescence, while the bottom bar compares the EGFP fluorescence to baseline distribution. Right: Direct EGFP fluorescence evoked by a single example ECS. Each panel shows the average calcium activity over a 10 ms window starting at the time indicated above the panel. (B)Low-passed EGFP fluorescence during an example ECS session with unilateral calcium event-like propagation over the right hemisphere. (C)Maximum $\Delta F/F_0$ during calcium and EGFP events. (D)Propagation speed of travelling events (Methods). Each data point is the median speed across one event.

Acknowledgements

We thank all the members of the Keller lab for discussion and support, Tingjia Lu and FMI vector core for AAV production, Jennifer Gröli for animal husbandry, and Felix Widmer for inspiration. Our work was supported by a team of core facilities at the FMI. The project has received funding from the Swiss National Science Foundation (GBK), the Novartis Research Foundation (GBK), EMBO postdoctoral fellowship ALTF 844-2022 (LL), and the European Research Council (ERC) under the European Union's Horizon 2020 research and innovation programme (grant agreement No 865617) (GBK).

Additional information

Author contributions

HL designed the study, performed the widefield calcium experiments and most data analysis. LS, LL, and HL performed the IEG experiments. HL and Ed. S performed the concurrent EEG and widefield calcium imaging experiments. LL, TK and HL performed the two photon imaging experiments. SU, El. S, GD, and AB performed the ECT treatment in patients and collected the data. All authors wrote the manuscript.

Funding

Funder	Grant reference number	Author
Swiss National Science Foundation		Georg B Keller
European Molecular Biology Organization (EMBO)	ALTF 844-2022	Leonardo Lupori
EC | European Research Council (ERC)	https://doi.org/10.3030/865617	Georg B Keller
Novartis Research Foundation		Georg B Keller

Author ORCID iDs

Georg B Keller: https://orcid.org/0000-0002-1401-0117

Additional files

Video S1. Widefield calcium imaging of a calcium event following ECS. Examples of ECS triggering a calcium event over the left hemisphere (left), both hemispheres (middle) and right hemisphere (right) in widefield calcium imaging.

Video S2. Two-photon calcium imaging of a calcium event following ECS. Examples of ECS triggering a calcium event while imaging upper L2/3 with two-photon calcium imaging.

Video S3. Two-photon micro-prism imaging of a calcium event following ECS. Examples of ECS triggering a calcium event while imaging all cortical layers through a micro-prism implant (see Methods).

References

Accornero F (1988) An Eyewitness Account of the Discovery of Electroshock. *J Ect* **4**:40 PubMed

Andermann ML, Gilfoy NB, Goldey GJ, Sachdev RNS, Wölfel M, McCormick DA, Reid RC, Levene MJ (2013) Chronic Cellular Imaging of Entire Cortical Columns in Awake Mice Using Microprisms. *Neuron* **80**:900-913 https://doi.org/10.1016/j.neuron.2013.07.052 | PubMed

Attinger A, Wang B, Keller GB (2017) Visuomotor Coupling Shapes the Functional Development of Mouse Visual Cortex. *Cell* **169**:1291-1302.e14. https://doi.org/10.1016/j.cell.2017.05.023 | PubMed

Baghai TC, Möller H.-J (2008) Electroconvulsive therapy and its different indications. *Dialogues Clin Neurosci* **10**:105-117 https://doi.org/10.31887/DCNS.2008.10.1/tcbaghai | PubMed

Bal T, Debay D, Destexhe A (2000) Cortical Feedback Controls the Frequency and Synchrony of Oscillations in the Visual Thalamus. *J Neurosci* **20**:7478-7488 https://doi.org/10.1523/JNEUROSCI.20-19-07478.2000 | PubMed

Baldinger P, Lotan A, Frey R, Kasper S, Lerer B, Lanzenberger R (2014) Neurotransmitters and Electroconvulsive Therapy. *J Ect* **30**:116 https://doi.org/10.1097/YCT.0000000000000138

Batiuk MY, Tyler T, Dragicevic K, Mei S, Rydbirk R, Petukhov V, Deviatiiarov R, Sedmak D, Frank E, Feher V, *et al.* (2022) Upper cortical layer–driven network impairment in schizophrenia. *Sci Adv* **8**:eabn8367 https://doi.org/10.1126/sciadv.abn8367 | PubMed

Benjamini Y, Hochberg Y (1995) Controlling the False Discovery Rate: A Practical and Powerful Approach to Multiple Testing. *J R Stat Soc Ser B Methodol* **57**:289-300 https://doi.org/10.1111/j.2517-6161.1995.tb02031.x

Bouckaert F, Sienaert P, Obbels J, Dols A, Vandenbulcke M, Stek M, Bolwig T (2014) ECT: Its Brain Enabling Effects: A Review of Electroconvulsive Therapy–Induced Structural Brain Plasticity. *J Ect* **30**:143 https://doi.org/10.1097/YCT.0000000000000129 | PubMed

Bracht T, Köhler L, Pfammatter M, Denier N, Soravia LM, Adorjan K, Hubl D, Draganski B, Olbrich S, Brühl A, *et al.* (2026) Hippocampal volume trajectory and its relation to clinical course during and following ECT-treatment in patients with depression: A systematic review and meta-analysis. *J Affect Disord* **402**:121344 https://doi.org/10.1016/j.jad.2026.121344 | PubMed

Brinley FJ, Kandel ER, Marshall WH (1960) Potassium outflux from rabbit cortex during spreading depression. *J Neurophysiol* **23**:246-256 https://doi.org/10.1152/jn.1960.23.3.246 | PubMed

Brumback RA, Staton RD (1982) The Electroencephalographic Pattern during Electroconvulsive Therapy. *Clin Electroencephalogr* **13**:148-153 https://doi.org/10.1177/155005948201300306

Buchanan KA, Blackman AV, Moreau AW, Elgar D, Costa RP, Lalanne T, Tudor Jones AA, Oyrer J, Sjöström PJ (2012) Target-Specific Expression of Presynaptic NMDA Receptors in Neocortical Microcircuits. *Neuron* **75**:451-466 https://doi.org/10.1016/j.neuron.2012.06.017 | PubMed

Casarotto PC, Girych M, Fred SM, Kovaleva V, Moliner R, Enkavi G, Biojone C, Cannarozzo C, Sahu MP, Kaurinkoski K, *et al.* (2021) Antidepressant drugs act by directly binding to TRKB neurotrophin receptors. *Cell* **184**:1299-1313.e19. https://doi.org/10.1016/j.cell.2021.01.034 | PubMed

Chan KY, Jang MJ, Yoo BB, Greenbaum A, Ravi N, Wu W.-L, Sánchez-Guardado L, Lois C, Mazmanian SK, Deverman BE, *et al.* (2017) Engineered AAVs for efficient noninvasive gene delivery to the central and peripheral nervous systems. *Nat Neurosci* **20**:1172-1179 https://doi.org/10.1038/nn.4593 | PubMed

Chen Q, Ren Li, Min Su, Hao Xuechao, Chen Hengsheng, Deng J (2018) Changes in synaptic plasticity are associated with electroconvulsive shock-induced learning and memory impairment in rats with depression-like behavior. *Neuropsychiatr Dis Treat* **14**:1737-1746 https://doi.org/10.2147/NDT.S163756 | PubMed

Cinderella MA, Nichols NA, Munjal S, Yan J, Kimball JN, Gligorovic P (2022) Antiepileptics in Electroconvulsive Therapy: A Mechanism-Based Review of Recent Literature. *J Ect* **38**:133 https://doi.org/10.1097/YCT.0000000000000805 | PubMed

Cole EJ, Phillips AL, Bentzley BS, Stimpson KH, Nejad R, Barmak F, Veerapal C, Khan N, Cherian K, Felber E, *et al.* (2022) Stanford Neuromodulation Therapy (SNT): A Double-Blind Randomized Controlled Trial. *Am J Psychiatry* **179**:132-141 https://doi.org/10.1176/appi.ajp.2021.20101429 | PubMed

Dehbandi S, Speckmann E.-J, Pape HC, Gorji A (2008) Cortical spreading depression modulates synaptic transmission of the rat lateral amygdala. *Eur J Neurosci* **27**:2057-2065 https://doi.org/10.1111/j.1460-9568.2008.06188.x | PubMed

Delva NJ, Brunet D, Hawken ER, Kesteven RM, Lawson JS, Lywood DW, Rodenburg M, Waldron JJ (2000) Electrical Dose and Seizure Threshold: Relations to Clinical Outcome and Cognitive Effects in Bifrontal, Bitemporal, and Right Unilateral ECT. *J Ect* **16**:361 https://doi.org/10.1097/00124509-200012000-00006 | PubMed

Deng Z.-D, Lisanby SH, Peterchev AV (2011) Electric field strength and focality in electroconvulsive therapy and magnetic seizure therapy: A finite element simulation study. *J Neural Eng* **8**:016007 https://doi.org/10.1088/1741-2560/8/1/016007 | PubMed

Deng Z.-D, Robins PL, Regenold W, Rohde P, Dannhauer M, Lisanby SH (2024) How electroconvulsive therapy works in the treatment of depression: is it the seizure, the electricity, or both?. *Neuropsychopharmacology* **49**:150-162 https://doi.org/10.1038/s41386-023-01677-2 | PubMed

Dreier JP, Major S, Pannek H.-W, Woitzik J, Scheel M, Wiesenthal D, Martus P, Winkler MKL, Hartings JA, Fabricius M, *et al.* (2012) Spreading convulsions, spreading depolarization and epileptogenesis in human cerebral cortex. *Brain* **135**:259-275 https://doi.org/10.1093/brain/awr303 | PubMed

Enger R, Tang W, Vindedal GF, Jensen V, Johannes Helm P, Sprengel R, Looger LL, Nagelhus EA (2015) Dynamics of Ionic Shifts in Cortical Spreading Depression. *Cereb Cortex N Y N 1991* **25**:4469-4476 https://doi.org/10.1093/cercor/bhv054 | PubMed

Estrada H, Robin J, Özbek A, Chen Z, Marowsky A, Zhou Q, Beck D, le Roy B, Arand M, Shoham S, *et al.* (2021) High-resolution fluorescence-guided transcranial ultrasound mapping in the live mouse brain. *Sci Adv* **7**:eabi5464 https://doi.org/10.1126/sciadv.abi5464 | PubMed

Faraguna U, Nelson A, Vyazovskiy VV, Cirelli C, Tononi G (2010) Unilateral cortical spreading depression affects sleep need and induces molecular and electrophysiological signs of synaptic potentiation in vivo. *Cereb Cortex* **20**:2939-2947 https://doi.org/10.1093/cercor/bhq041 | PubMed

Francis-Taylor R, Ophel G, Martin D, Loo C (2020) The ictal EEG in ECT: A systematic review of the relationships between ictal features, ECT technique, seizure threshold and outcomes. *Brain Stimulat* **13**:1644-1654 https://doi.org/10.1016/j.brs.2020.09.009 | PubMed

Fregni F, Liebetanz D, Monte-Silva KK, Oliveira MB, Santos AA, Nitsche MA, Pascual-Leone A, Guedes RCA (2007) Effects of transcranial direct current stimulation coupled with repetitive electrical stimulation on cortical spreading depression. *Exp Neurol* **204**:462-466 https://doi.org/10.1016/j.expneurol.2006.09.019 | PubMed

Freundlieb N, Schneider E, Brühl A, Kiebs M (2023) GENET-GPD: A documentation tool to digitally collect longitudinal ECT treatment data and associated biosignals. *Brain Stimulat* **16**:1173-1175 https://doi.org/10.1016/j.brs.2023.07.053 | PubMed

Gillving C, Ekman CJ, Hammar Å, Landén M, Lundberg J, Movahed Rad P, Nordanskog P, von Knorring L, Nordenskjöld A (2024) Seizure Duration and Electroconvulsive Therapy in Major Depressive Disorder. *JAMA Netw Open* **7**:e2422738 https://doi.org/10.1001/jamanetworkopen.2024.22738 | PubMed

Gongwer MW, Qi A, Enos AS, Rueda SA, Klune CB, Shari M, Kashay AQ, Williams OH, Hacking A, Riley JP, *et al.* (2025) A cell type-specific mechanism driving the rapid antidepressant effects of transcranial magnetic stimulation. *bioRxiv* 2025.01.29.635537 https://doi.org/10.1101/2025.01.29.635537

Grover S, Sahoo S, Rabha A, Koirala R (2019) ECT in schizophrenia: a review of the evidence. *Acta Neuropsychiatr* **31**:115-127 https://doi.org/10.1017/neu.2018.32 | PubMed

Grözinger M, Conca A, Nickl-Jockschat T, Di Pauli J (2013) *Elektrokonvulsionstherapie kompakt: Für Zuweiser und Anwender* Berlin, Heidelberg: Springer. https://doi.org/10.1007/978-3-642-25629-5

Haddad PM, Correll CU (2018) The acute efficacy of antipsychotics in schizophrenia: a review of recent meta-analyses. *Ther Adv Psychopharmacol* **8**:303-318 https://doi.org/10.1177/2045125318781475 | PubMed

Hadjikhani N, Sanchez del Rio M, Wu O, Schwartz D, Bakker D, Fischl B, Kwong KK, Cutrer FM, Rosen BR, Tootell RBH, *et al.* (2001) Mechanisms of migraine aura revealed by functional MRI in human visual cortex. *Proc Natl Acad Sci* **98**:4687-4692 https://doi.org/10.1073/pnas.071582498 | PubMed

Hagen E, Shprung D, Minakova E, Washington J, Kumar U, Shin D, Sankar R, Mazarati A (2015) Autism-Like Behavior in BTBR Mice Is Improved by Electroconvulsive Therapy. *Neurotherapeutics* **12**:657-666 https://doi.org/10.1007/s13311-015-0357-7 | PubMed

Dreier JP, Fabricius M, Ayata C, Sakowitz OW, Shuttleworth CW, Dohmen C, Graf R, Vajkoczy P, Helbok R, Suzuki M, *et al.* (2017) Recording, analysis, and interpretation of spreading depolarizations in neurointensive care: Review and recommendations of the COSBID research group. *J Cereb Blood Flow Metab* **37**:1595-1625 https://doi.org/10.1177/0271678X16654496 | PubMed

Heindorf M, Arber S, Keller GB (2018) Mouse Motor Cortex Coordinates the Behavioral Response to Unpredicted Sensory Feedback. *Neuron* **99**:1040-1054.e5. https://doi.org/10.1016/j.neuron.2018.07.046 | PubMed

Heindorf M, Keller GB (2024) Antipsychotic drugs selectively decorrelate long-range interactions in deep cortical layers. *eLife* **12** https://doi.org/10.7554/eLife.86805.3

Herreras O, Largo C, Ibarz JM, Somjen GG, Rio RM. del (1994) Role of neuronal synchronizing mechanisms in the propagation of spreading depression in the in vivo hippocampus. *J Neurosci* **14**:7087-7098 https://doi.org/10.1523/JNEUROSCI.14-11-07087.1994 | PubMed

Hofmeijer J, van Kaam CR, van de Werff B, Vermeer SE, Tjepkema-Cloostermans MC, van Putten MJAM (2018) Detecting Cortical Spreading Depolarization with Full Band Scalp Electroencephalography: An Illusion?. *Front Neurol* **9** https://doi.org/10.3389/fneur.2018.00017 | PubMed

Hogan RE, Trammel ER, Farber NB, Avidan MS, Palanca BJA (2019) Central-Positive Complexes: A Novel Characterization of Ictal Markers Induced During Electroconvulsive Therapy. *J Ect* **35**:e39 https://doi.org/10.1097/YCT.0000000000000597 | PubMed

Huels ER, Kafashan M, Hickman LB, Ching S, Lin N, Lenze EJ, Farber NB, Avidan MS, Hogan RE, Palanca BJA (2023) Central-positive complexes in ECT-induced seizures: Possible evidence for thalamocortical mechanisms. *Clin Neurophysiol Off J Int Fed Clin Neurophysiol* **146**:77-86 https://doi.org/10.1016/j.clinph.2022.11.015 | PubMed

Impastato DJ, Almansi R (1942) The electrofit in the treatment of mental disease. *J Nerv Ment Dis* **96**:395

Iqbal Chowdhury GM, Liu Y, Tanaka M, Fujioka T, Ishikawa A, Nakamura S (2003) Cortical spreading depression affects Fos expression in the hypothalamic paraventricular nucleus and the cerebral cortex of both hemispheres. *Neurosci Res* **45**:149-155 https://doi.org/10.1016/S0168-0102(02)00207-9 | PubMed

Joshi SH, Espinoza RT, Pirnia T, Shi J, Wang Y, Ayers B, Leaver A, Woods RP, Narr KL (2016) Structural Plasticity of the Hippocampus and Amygdala Induced by Electroconvulsive Therapy in Major Depression. *Biol Psychiatry, Depression: Neural Mechanisms of Treatment* **79**:282-292 https://doi.org/10.1016/j.biopsych.2015.02.029 | PubMed

Karatas H, Erdener SE, Gursoy-Ozdemir Y, Lule S, Eren-Koçak E, Sen ZD, Dalkara T (2013) Spreading depression triggers headache by activating neuronal Panx1 channels. *Science* **339**:1092-1095 https://doi.org/10.1126/science.1231897 | PubMed

Kauvar IV, Machado TA, Yuen E, Kochalka J, Choi M, Allen WE, Wetzstein G, Deisseroth K (2020) Cortical Observation by Synchronous Multifocal Optical Sampling Reveals Widespread Population Encoding of Actions. *Neuron* **107**:351-367.e19. https://doi.org/10.1016/j.neuron.2020.04.023 | PubMed

Keller GB, Bonhoeffer T, Hübener M (2012) Sensorimotor Mismatch Signals in Primary Visual Cortex of the Behaving Mouse. *Neuron* **74**:809-815 https://doi.org/10.1016/j.neuron.2012.03.040 | PubMed

Keller GB, Sterzer P (2024) Predictive Processing: A Circuit Approach to Psychosis. *Annu Rev Neurosci* **47**:85-101 https://doi.org/10.1146/annurev-neuro-100223-121214 | PubMed

Kellner CH (2018) *Handbook of ECT: A Guide to Electroconvulsive Therapy for Practitioners* Cambridge University Press.

Kelly ME, Battye RA, McIntyre DC (1999) Cortical spreading depression reversibly disrupts convulsive motor seizure expression in amygdala-kindled rats. *Neuroscience* **91**:305-313 https://doi.org/10.1016/S0306-4522(98)00656-3 | PubMed

Kim SH, Yu HS, Huh S, Kang UG, Kim YS (2022) Electroconvulsive seizure inhibits the mTOR signaling pathway via AMPK in the rat frontal cortex. *Psychopharmacology* **239**:443-454 https://doi.org/10.1007/s00213-021-06015-2 | PubMed

Kim TH, Zhang Y, Lecoq J, Jung JC, Li J, Zeng H, Niell CM, Schnitzer MJ (2016) Long-Term Optical Access to an Estimated One Million Neurons in the Live Mouse Cortex. *Cell Rep* **17**:3385-3394 https://doi.org/10.1016/j.celrep.2016.12.004 | PubMed

Kimball JN, Rosenquist PB, Dunn A, McCall V (2009) Prediction of antidepressant response in both 2.25 × threshold RUL and fixed high dose RUL ECT. *J Affect Disord* **112**:85-91 https://doi.org/10.1016/j.jad.2008.03.030 | PubMed

Kneen M, Farinas J, Li Y, Verkman AS (1998) Green fluorescent protein as a noninvasive intracellular pH indicator. *Biophys J* **74**:1591-1599 https://doi.org/10.1016/S0006-3495(98)77870-1 | PubMed

Krystal AD, Weiner RD (1994) ECT Seizure Therapeutic Adequacy. *J Ect* **10**:153 PubMed

Krystal AD, Weiner RD, Coffey CE (1995) The ictal EEG as a marker of adequate stimulus intensity with unilateral ECT. *J Neuropsychiatry Clin Neurosci* **7**:295-303 https://doi.org/10.1176/jnp.7.3.295 | PubMed

Larsen MH, Olesen M, Woldbye DPD, Hay-Schmidt A, Hansen HH, Rønn LCB, Mikkelsen JD (2005) Regulation of activity-regulated cytoskeleton protein (*Arc*) mRNA after acute and chronic electroconvulsive stimulation in the rat. *Brain Res* **1064**:161-165 https://doi.org/10.1016/j.brainres.2005.09.039 | PubMed

Lauritzen M, Dreier JP, Fabricius M, Hartings JA, Graf R, Strong AJ (2011) Clinical relevance of cortical spreading depression in neurological disorders: migraine, malignant stroke, subarachnoid and intracranial hemorrhage, and traumatic brain injury. *J Cereb Blood Flow Metab Off J Int Soc Cereb Blood Flow Metab* **31**:17-35 https://doi.org/10.1038/jcbfm.2010.191 | PubMed

Leao AAP (1944) Spreading depression of activity in the cerebral cortex. *J Neurophysiol* **7**:359-390 https://doi.org/10.1152/jn.1944.7.6.359

Lein ES, Hawrylycz MJ, Ao N, Ayres M, Bensinger A, Bernard A, Boe AF, Boguski MS, Brockway KS, Byrnes EJ, *et al.* (2007) Genome-wide atlas of gene expression in the adult mouse brain. *Nature* **445**:168-176 https://doi.org/10.1038/nature05453 | PubMed

Leinweber M, Zmarz P, Buchmann P, Argast P, Hübener M, Bonhoeffer T, Keller GB (2014) Two-photon Calcium Imaging in Mice Navigating a Virtual Reality Environment. *J Vis Exp* 1-6 https://doi.org/10.3791/50885 | PubMed

Leo AAP, Morison RS (1945) Propagation of spreading cortical depression. *J Neurophysiol* **8**:33-45 https://doi.org/10.1152/jn.1945.8.1.33

Li B, Zhou F, Luo Q, Li P (2012) Altered resting-state functional connectivity after cortical spreading depression in mice. *NeuroImage* **63**:1171-1177 https://doi.org/10.1016/j.neuroimage.2012.08.024 | PubMed

Lupori L, Heindorf M, Kouvaros S, Schildkamp A, Bischofberger J, Keller GB (2026) A single dose of the antipsychotic drug clozapine has long-term behavioral and functional effects in mice. *bioRxiv* 2026.03.27.714783 https://doi.org/10.64898/2026.03.27.714783

Lupori L, Totaro V, Cornuti S, Ciampi L, Carrara F, Grilli E, Viglione A, Tozzi F, Putignano E, Mazziotti R, *et al.* (2023) A comprehensive atlas of perineuronal net distribution and colocalization with parvalbumin in the adult mouse brain. *Cell Rep* **42** https://doi.org/10.1016/j.celrep.2023.112788 | PubMed

Ma Y, Shaik MA, Kim SH, Kozberg MG, Thibodeaux DN, Zhao HT, Yu H, Hillman EMC (2016) Wide-field optical mapping of neural activity and brain haemodynamics: considerations and novel approaches. *Philos Trans R Soc B Biol Sci* **371**:20150360 https://doi.org/10.1098/rstb.2015.0360 | PubMed

Mahringer D, Petersen A, Fiser A, Okuno H, Bito H, Perrier J.-F, Keller G (2019) Expression of c-Fos and Arc in hippocampal region CA1 marks neurons that exhibit learning-related activity changes. *bioRxiv* 644526 https://doi.org/10.1101/644526

Mahringer D, Zmarz P, Okuno H, Bito H, Keller GB (2022) Functional correlates of immediate early gene expression in mouse visual cortex. *Peer Community J* **2** https://doi.org/10.24072/pcjournal.156 | PubMed

Martin JL, Strawbridge RJ, Christmas D, Fleming M, Kelly S, Varveris D, Martin D (2025) Electroconvulsive Therapy: A Scotland-Wide Naturalistic Study of 4826 Treatment Episodes. *Biol Psychiatry Glob Open Sci* **5**:100434 https://doi.org/10.1016/j.bpsgos.2024.100434 | PubMed

Mazel T, Richter F, Vargová L, Syková E (2002) Changes in extracellular space volume and geometry induced by cortical spreading depression in immature and adult rats. *Physiol Res* **51**:S85-93 https://doi.org/10.33549/physiolres.930000.51.s85 | PubMed

McCormick LM, Boles Ponto LL, Pierson RK, Johnson HJ, Magnotta V, Brumm MC (2007) Metabolic Correlates of Antidepressant and Antipsychotic Response in Patients With Psychotic Depression Undergoing Electroconvulsive Therapy. *J Ect* **23**:265 https://doi.org/10.1097/yct.0b013e318150d56d | PubMed

Meeren HKM, Pijn JPM, Luijtelaar ELJMV, Coenen AML, Silva FHL. da (2002) Cortical Focus Drives Widespread Corticothalamic Networks during Spontaneous Absence Seizures in Rats. *J Neurosci* **22**:1480-1495 https://doi.org/10.1523/JNEUROSCI.22-04-01480.2002 | PubMed

Mitlasóczki B, Gutiérrez Gómez A, Kamali M, Babushkina N, Baues M, Kück L, Haubrich AN, Tamiolakis T, Breuer A, Granak S, *et al.* (2025) Hippocampal spreading depolarization as a driver of postictal ambulation. *Sci Transl Med* **17**:eadv3260 https://doi.org/10.1126/scitranslmed.adv3260 | PubMed

Mulder LAC, Grootens KP (2020) The Incidence of Post-Electroconvulsive Therapy Headache: A Systematic Review. *J Ect* **36**:e22-e28 https://doi.org/10.1097/YCT.0000000000000677 | PubMed

Mutel V, Buchy D, Klingelschmidt A, Messer J, Bleuel Z, Kemp JA, Richards JG (1998) In vitro binding properties in rat brain of [3H]Ro 25-6981, a potent and selective antagonist of NMDA receptors containing NR2B subunits. *J Neurochem* **70**:2147-2155 https://doi.org/10.1046/j.1471-4159.1998.70052147.x | PubMed

Nanou E, Catterall WA (2018) Calcium Channels, Synaptic Plasticity, and Neuropsychiatric Disease. *Neuron* **98**:466-481 https://doi.org/10.1016/j.neuron.2018.03.017 | PubMed

Nasretdinov A, Vinokurova D, Lemale CL, Burkhanova-Zakirova G, Chernova K, Makarova J, Herreras O, Dreier JP, Khazipov R (2023) Diversity of cortical activity changes beyond depression during Spreading Depolarizations. *Nat Commun* **14**:7729 https://doi.org/10.1038/s41467-023-43509-3 | PubMed

Nobler MS, Sackeim HA, Solomou M, Luber B, Devanand DP, Prudic J (1993) EEG manifestations during ECT: effects of electrode placement and stimulus intensity. *Biol Psychiatry* **34**:321-330 https://doi.org/10.1016/0006-3223(93)90089-V | PubMed

Oh J, Ryu JS, Kim J, Kim S, Jeong HS, Kim KR, Kim H.-C, Yoo S.-S, Seok J.-H (2024) Effect of Low-Intensity Transcranial Focused Ultrasound Stimulation in Patients With Major Depressive Disorder: A Randomized, Double-Blind, Sham-Controlled Clinical Trial. *Psychiatry Investig* **21**:885-896 https://doi.org/10.30773/pi.2024.0016 | PubMed

Pandya CD, Kutiyanawalla A, Pillai A (2013) BDNF-TrkB Signaling and Neuroprotection in Schizophrenia. *Asian J Psychiatry* **6**:22-28 https://doi.org/10.1016/j.ajp.2012.08.010 | PubMed

Perera TD, Luber B, Nobler MS, Prudic J, Anderson C, Sackeim HA (2004) Seizure Expression During Electroconvulsive Therapy: Relationships with Clinical Outcome and Cognitive Side Effects. *Neuropsychopharmacology* **29**:813-825 https://doi.org/10.1038/sj.npp.1300377 | PubMed

Perugi G, Medda P, Toni C, Mariani MG, Socci C, Mauri M (2017) The Role of Electroconvulsive Therapy (ECT) in Bipolar Disorder: Effectiveness in 522 Patients with Bipolar Depression, Mixed-state, Mania and Catatonic Features. *Curr Neuropharmacol* **15**:359-371 https://doi.org/10.2174/1570159X14666161017233642 | PubMed

Peterchev AV, Krystal AD, Rosa MA, Lisanby SH (2015) Individualized Low-Amplitude Seizure Therapy: Minimizing Current for Electroconvulsive Therapy and Magnetic Seizure Therapy. *Neuropsychopharmacology* **40**:2076-2084 https://doi.org/10.1038/npp.2015.122 | PubMed

Peterchev AV, Rosa MA, Deng Z.-D, Prudic J, Lisanby Sarah.H (2010) ECT Stimulus Parameters: Rethinking Dosage. *J Ect* **26**:159-174 https://doi.org/10.1097/YCT.0b013e3181e48165 | PubMed

Petrides G, Fink M, Husain MM, Knapp RG, Rush AJ, Mueller M, Rummans TA, O'Connor KM, Rasmussen KG, Bernstein HJ, *et al.* (2001) ECT remission rates in psychotic versus nonpsychotic depressed patients: a report from CORE. *J Ect* **17**:244-253 https://doi.org/10.1097/00124509-200112000-00003 | PubMed

Pietrobon D, Moskowitz MA (2014) Chaos and commotion in the wake of cortical spreading depression and spreading depolarizations. *Nat Rev Neurosci* **15**:379-393 https://doi.org/10.1038/nrn3770 | PubMed

Polack P.-O, Mahon S, Chavez M, Charpier S (2009) Inactivation of the Somatosensory Cortex Prevents Paroxysmal Oscillations in Cortical and Related Thalamic Neurons in a Genetic Model of Absence Epilepsy. *Cereb Cortex* **19**:2078-2091 https://doi.org/10.1093/cercor/bhn237 | PubMed

Porter RJ, Baune BT, Morris G, Hamilton A, Bassett D, Boyce P, Hopwood MJ, Mulder R, Parker G, Singh AB, *et al.* (2020) Cognitive side-effects of electroconvulsive therapy: what are they, how to monitor them and what to tell patients. *BJPsych Open* **6**:e40 https://doi.org/10.1192/bjo.2020.17 | PubMed

Pottkämper JCM, Verdijk JPAJ, Hofmeijer J, van Waarde JA, van Putten MJAM (2021) Seizures induced in electroconvulsive therapy as a human epilepsy model: A comparative case study. *Epilepsia Open* **6**:672-684 https://doi.org/10.1002/epi4.12532 | PubMed

Ramnauth AD, Maynard KR, Kardian AS, Phan BN, Tippani M, Rajpurohit S, Hobbs JW, Cerceo Page S, Jaffe AE, Martinowich K (2022) Induction of Bdnf from promoter I following electroconvulsive seizures contributes to structural plasticity in neurons of the piriform cortex. *Brain Stimulat* **15**:427-433 https://doi.org/10.1016/j.brs.2022.02.003 | PubMed

Rosenthal ZP, Majeski JB, Somarowthu A, Quinn DK, Lindquist BE, Putt ME, Karaj A, Favilla CG, Baker WB, Hosseini G, *et al.* (2025) Electroconvulsive therapy generates a postictal wave of spreading depolarization in mice and humans. *Nat Commun* **16**:4619 https://doi.org/10.1038/s41467-025-59900-1 | PubMed

Sackeim HA, Decina P, Portnoy S, Neeley P, Malitz S (1987) Studies of dosage, seizure threshold, and seizure duration in ECT. *Biol Psychiatry* **22**:249-268 https://doi.org/10.1016/0006-3223(87)90144-2 | PubMed

Sackeim HA, Devanand DP, Prudic J (1991) Stimulus Intensity, Seizure Threshold, and Seizure Duration: Impact on the Efficacy and Safety of Electroconvulsive Therapy. *Psychiatr Clin* **14**:803-843 https://doi.org/10.1016/S0193-953X(18)30271-5 | PubMed

Sackeim HA, Prudic J, Fuller R, Keilp J, Lavori PW, Olfson M (2007) The cognitive effects of electroconvulsive therapy in community settings. *Neuropsychopharmacol Off Publ Am Coll Neuropsychopharmacol* **32**:244-254 https://doi.org/10.1038/sj.npp.1301180 | PubMed

Saravanan V, Berman GJ, Sober SJ (2020) Application of the hierarchical bootstrap to multi-level data in neuroscience. *Neurons Behav Data Anal Theory* **3** PubMed

Sawant-Pokam PM, Suryavanshi P, Mendez JM, Dudek FE, Brennan KC (2017) Mechanisms of Neuronal Silencing After Cortical Spreading Depression. *Cereb Cortex* **27**:bhv328 https://doi.org/10.1093/cercor/bhv328 | PubMed

Scharfman HE (2002) Epilepsy as an Example of Neural Plasticity. *Neurosci Rev J Bringing Neurobiol Neurol Psychiatry* **8**:154-173 https://doi.org/10.1177/107385840200800211 | PubMed

Scholkmann F, Boss J, Wolf M (2012) An Efficient Algorithm for Automatic Peak Detection in Noisy Periodic and Quasi-Periodic Signals. *Algorithms* **5**:588-603 https://doi.org/10.3390/a5040588

Seidel JL, Escartin C, Ayata C, Bonvento G, Shuttleworth CW (2016) Multifaceted roles for astrocytes in spreading depolarization: A target for limiting spreading depolarization in acute brain injury?. *Glia* **64**:5-20 https://doi.org/10.1002/glia.22824 | PubMed

Shao L.-X, Liao C, Davoudian PA, Savalia NK, Jiang Q, Wojtasiewicz C, Tan D, Nothnagel JD, Liu R.-J, Woodburn SC, *et al.* (2025) Psilocybin's lasting action requires pyramidal cell types and 5-HT2A receptors. *Nature* **642**:411-420 https://doi.org/10.1038/s41586-025-08813-6 | PubMed

Siegle JH, López AC, Patel YA, Abramov K, Ohayon S, Voigts J (2017) Open Ephys: an open-source, plugin-based platform for multichannel electrophysiology. *J Neural Eng* **14**:045003 https://doi.org/10.1088/1741-2552/aa5eea | PubMed

Singh A, Kar SK (2017) How Electroconvulsive Therapy Works?: Understanding the Neurobiological Mechanisms. *Clin Psychopharmacol Neurosci* **15**:210-221 https://doi.org/10.9758/cpn.2017.15.3.210 | PubMed

Somjen GG (2001) Mechanisms of Spreading Depression and Hypoxic Spreading Depression-Like Depolarization. *Physiol Rev* **81**:1065-1096 https://doi.org/10.1152/physrev.2001.81.3.1065 | PubMed

Sowers LP, Massey CA, Gehlbach BK, Granner MA, Richerson GB (2013) Sudden unexpected death in epilepsy: Fatal post-ictal respiratory and arousal mechanisms. *Respir Physiol Neurobiol* **189**:315-323 https://doi.org/10.1016/j.resp.2013.05.010 | PubMed

Stafstrom CE (2020) Stopped At the Border: Cortical Spreading Depolarization Blocks Seizure Propagation. *Epilepsy Curr* **20**:171-172 https://doi.org/10.1177/1535759720916448 | PubMed

Stern MA, Cole ER, Gutekunst C.-A, Yang JJ, Berglund K, Gross RE (2024) Organellular imaging in vivo reveals a depletion of endoplasmic reticular calcium during post-ictal cortical spreading depolarization. *bioRxiv* https://doi.org/10.1101/2024.09.21.614252 | PubMed

Stuiver S, Tewarie PKB, Pottkämper JCM, Verdijk JPAJ, van Putten MJAM, Hofmeijer J, van Waarde JA (2026) Temporal dynamics of electroconvulsive therapy induced seizures. *Clin Neurophysiol* **181**:2111439 https://doi.org/10.1016/j.clinph.2025.2111439 | PubMed

Sun X, Wang Y, Chen S, Luo W, Li P, Luo Q (2011) Simultaneous monitoring of intracellular pH changes and hemodynamic response during cortical spreading depression by fluorescence-corrected multimodal optical imaging. *NeuroImage* **57**:873-884 https://doi.org/10.1016/j.neuroimage.2011.05.040 | PubMed

Takamiya A, Riemer F, Erchinger VJ, Korbmacher M, Bartsch H, Ousdal OT, Maximov I, Dale A, Emsell L, Oedegaard KJ, *et al.* (2025) Acute and transient change in brain water content induced by a single electroconvulsive therapy session. *Brain Stimulat* **18**:2008-2015 https://doi.org/10.1016/j.brs.2025.10.021 | PubMed

Takano H, Motohashi N, Uema T, Ogawa K, Ohnishi T, Nishikawa M, Matsuda H (2011) Differences in cerebral blood flow between missed and generalized seizures with electroconvulsive therapy: A positron emission tomographic study. *Epilepsy Res* **97**:225-228 https://doi.org/10.1016/j.eplepsyres.2011.08.007 | PubMed

Takano T, Tian G.-F, Peng W, Lou N, Lovatt D, Hansen AJ, Kasischke KA, Nedergaard M (2007) Cortical spreading depression causes and coincides with tissue hypoxia. *Nat Neurosci* **10**:754-762 https://doi.org/10.1038/nn1902 | PubMed

American Psychiatric Association (2025) *The Practice of Electroconvulsive Therapy* (Third Edition) American Psychiatric Association.

Tor PC, Tan XW, Martin D, Loo C (2021) Comparative outcomes in electroconvulsive therapy (ECT): A naturalistic comparison between outcomes in psychosis, mania, depression, depression and catatonia. *Psychotic Eur Neuropsychopharmacol J Eur CollNeuropsychopharmacol* **51**:43-54 https://doi.org/10.1016/j.euroneuro.2021.04.023 | PubMed

Trifu S, Sevcenco A, Stănescu M, Drăgoi AM, Cristea MB (2021) Efficacy of electroconvulsive therapy as a potential first-choice treatment in treatment-resistant depression (Review). *Exp Ther Med* **22**:1281 https://doi.org/10.3892/etm.2021.10716 | PubMed

Ulett GA, Smith K, Gleser GC (1956) Evaluation of convulsive and subconvulsive shock therapies utilizing a control group. *Am J Psychiatry* **112**:795-802 https://doi.org/10.1176/ajp.112.10.795 | PubMed

Ulrich S, Schneider E, Deuring G, Erni S, Ridder M, Sarlon J, Brühl AB (2025) Alterations in resting-state EEG functional connectivity in patients with major depressive disorder receiving electroconvulsive therapy: A systematic review. *Neurosci Biobehav Rev* **169**:106017 https://doi.org/10.1016/j.neubiorev.2025.106017 | PubMed

van Buel EM, Sigrist H, Seifritz E, Fikse L, Bosker FJ, Schoevers RA, Klein HC, Pryce CR, Eisel UL (2017) Mouse repeated electroconvulsive seizure (ECS) does not reverse social stress effects but does induce behavioral and hippocampal changes relevant to electroconvulsive therapy (ECT) side-effects in the treatment of depression. *PLoS ONE* **12**:e0184603 https://doi.org/10.1371/journal.pone.0184603 | PubMed

Verdijk JPAJ, van Dijk-Schouten TAL, Pottkämper JCM, van de Mortel LA, ten Doesschate F, Stuiver S, Chamberland M, Norris DG, van Putten MJAM, Hofmeijer J, *et al.* (2026) Postictal agitation is associated with brain-wide postictal microstructural changes after electroconvulsive therapy-induced seizures. *Brain Stimulat* **19**:103031 https://doi.org/10.1016/j.brs.2026.103031 | PubMed

Vesuna S, Kauvar IV, Richman E, Gore F, Oskotsky T, Sava-Segal C, Luo L, Malenka RC, Henderson JM, Nuyujukian P, *et al.* (2020) Deep posteromedial cortical rhythm in dissociation. *Nature* **586**:87-94 https://doi.org/10.1038/s41586-020-2731-9 | PubMed

Wang Q, Ding S.-L, Li Y, Royall J, Feng D, Lesnar P, Graddis N, Naeemi M, Facer B, Ho A, *et al.* (2020) The Allen Mouse Brain Common Coordinate Framework: A 3D Reference Atlas. *Cell* **181**:936-953.e20. https://doi.org/10.1016/j.cell.2020.04.007 | PubMed

Watanabe Y, Johnson RS, Butler LS, Binder DK, Spiegelman BM, Papaioannou VE, McNamara JO (1996) Null Mutation of c-fos Impairs Structural and Functional Plasticities in the Kindling Model of Epilepsy. *J Neurosci* **16**:3827-3836 https://doi.org/10.1523/JNEUROSCI.16-12-03827.1996 | PubMed

Wei Q, Bai T, Brown EC, Xie W, Chen Y, Ji G, Ramasubbu R, Tian Y, Wang K (2020) Thalamocortical connectivity in electroconvulsive therapy for major depressive disorder. *J Affect Disord* **264**:163-171 https://doi.org/10.1016/j.jad.2019.11.120 | PubMed

Wernsmann B, Pape H.-C, Speckmann E.-J, Gorji A (2006) Effect of cortical spreading depression on synaptic transmission of rat hippocampal tissues. *Eur J Neurosci* **23**:1103-1110 https://doi.org/10.1111/j.1460-9568.2006.04643.x | PubMed

Wilkinson ST, Sanacora G, Bloch MH (2017) Hippocampal volume changes following electroconvulsive therapy: a systematic review and meta-analysis. *Biol Psychiatry Cogn Neurosci Neuroimaging* **2**:327-335 https://doi.org/10.1016/j.bpsc.2017.01.011 | PubMed

Yang G, Pan F, Parkhurst CN, Grutzendler J, Gan W.-B (2010) Thinned-skull cranial window technique for long-term imaging of the cortex in live mice. *Nat Protoc* **5**:201-208 https://doi.org/10.1038/nprot.2009.222 | PubMed

Yogesh B, Heindorf M, Jordan R, Keller GB (2025) Quantification of the effect of hemodynamic occlusion in two-photon imaging of mouse cortex. *eLife* **14**:RP104914 https://doi.org/10.7554/eLife.104914 | PubMed

Zakharov A, Chernova K, Burkhanova G, Holmes GL, Khazipov R (2019) Segregation of seizures and spreading depolarization across cortical layers. *Epilepsia* **60**:2386-2397 https://doi.org/10.1111/epi.16390 | PubMed

Zhou N, Rungta RL, Malik A, Han H, Wu DC, MacVicar BA (2013) Regenerative Glutamate Release by Presynaptic NMDA Receptors Contributes to Spreading Depression. *J Cereb Blood Flow Metab* **33**:1582-1594 https://doi.org/10.1038/jcbfm.2013.113 | PubMed

Peer reviews

Reviewer #1 (Public review):

The work corroborates the idea, recently suggested by Rosenthal et al. (2025), that spreading depolarization is involved in the mechanisms of electroconvulsive therapy. Using a mouse

model of electroconvulsive therapy and various sophisticated approaches to visualize cortical activity, the authors provide an extensive description of traveling calcium waves induced by electroconvulsive stimulation. The study confirms that the calcium events have properties typical of cortical spreading depolarization and seeks to show that the calcium/SD waves mediate therapeutic and neuroplastic effects of electroconvulsive therapy. The authors find that after electroconvulsive stimulation associated with calcium/SD waves, Fos expression increases widely; in the cortex, this increase is localized to the hemisphere affected by calcium waves. They show that some EEG predictors of the beneficial effects of electroconvulsive therapy correlate with the occurrence of calcium/SD waves. Despite the solid methodology and the study's interesting, its conclusions are not fully supported by the data.

In particular:

(1)The title of the paper claims that "electroconvulsive stimulation drives cortical spreading depolarization dependent immediate early gene expression". However, immunohistochemical staining shows that Fos expression increases not only in the cortex but also in many subcortical regions, including the hippocampus and amygdala (Figure 5A). Really, conventional electroconvulsive therapy stimulates nearly the entire brain volume and induces generalized seizure activity that can trigger SD not only in the cortex but also in other brain sites. Therefore, regions beyond the cortex can also drive the effects of electroconvulsive therapy. Next, the authors use Fos staining as a marker of neuronal plasticity. However, Fos is also a marker of preceding neuronal activation. As electroconvulsive stimulation, seizures, and SD are associated with high neural activity, it is unclear whether the observed Fos upregulation results from the prior activation or heralds the subsequent plastic changes. Other markers of neuroplasticity (e.g., BDNF) should also be examined.

(2) Postictal EEG suppression is one of the most promising correlates of positive clinical outcomes after electroconvulsive therapy. Cortical SD is also tightly coupled with suppression of neuronal activity in affected regions. Although the authors report that postictal suppression is stronger after stimulations with cortical SDs than without SDs, the cortices affected (ipsi) and unaffected (contra) by unilateral cortical calcium/SD events exhibit identical suppression (Figure 6F). The result contradicts established knowledge in the field. If the calcium events are cortical SDs, they should induce EEG suppression only in the affected hemisphere.

(3) The study states a beneficial role of calcium/SD waves in ECS effects. However, SD alters numerous aspects of brain function, leading to a range of effects that can underlie side effects as well. Assessment of the behavioral effects of stimulation with and without calcium/SD waves can help clarify the issue.

The results of the work suggest that cortical SD can contribute to electroconvulsive therapy-related mechanisms and help to optimize the stimulation parameters to achieve maximal therapeutic effect.

https://doi.org/10.7554/eLife.111896.1.sa2

Reviewer #2 (Public review):

Summary:

This manuscript addresses the question of mechanisms underlying the therapeutic effects of electroconvulsive therapy (ECT). Clinical efficacy of ECT in major depression (and other disorders) is well established and has often been assumed to be a direct consequence of seizure activity generated by the current application. However, as the authors point out, this

explanation is unsatisfactory. A recent study (Rosenthal et al., 2025) provided evidence that ECT generates a wave of cortical spreading depolarization (CSD) in mice, and initial evidence that similar events were generated in patients undergoing ECT. Based on their observations, Rosenthal et al. proposed that CSD, rather than seizure, may engage plasticity mechanisms that contribute to the brain's clinical response to ECT. The current study adds to that prior work by reporting other consequences of CSD, in addition to sustained Ca2+ elevations. The current study also links EEG characteristics immediately following the ECT with the likelihood of generating a CSD, which can help optimize ECT parameters.

Strengths:

An important research topic, linking a large set of rodent studies with a limited clinical EEG data set.

The data acquisition and analyses appear to be of very high quality, and the main results are well illustrated.

Association between EEG characteristics linked to good clinical outcome matched by mouse EEG data linked to CSD.

Characterization of multiple consequences of CSD following ECT in the mouse brain.

Weaknesses:

The main characterization of CSD propagation comes from GCaMP Ca2+ measurements, as previously reported (Rosenthal et al., 2025). That prior study also provided key electrophysiological evidence of CSD with a DC shift after ECT in mice (supplemental data). Given the prior evidence for ECT-CSD, the additional measures shown in the current manuscript are fully expected. Thus, the 2-photon imaging of Ca2+ elevations following CSD (Figure 4) is consistent with prior 2-photon imaging studies of CSD, and the complex hemodynamic and pH changes are expected to contribute to propagation of EGFP fluorescence changes (Supplemental Figure 5). These data are well presented, but, contrary to the results section here, these results appear confirmatory rather than necessary to build a case that the key event generated by ECT is a CSD.

The authors state that "our conclusion that CSD is the primary driver of plasticity is based on its role in driving Fos expression" (line 472). Related to the point above, there is already a very well-established literature showing that CSD leads to rapid and robust Fos expression in rodent cortex, so this is fully consistent with prior work. The prior work, CSD-fos work, should be summarized and/or cited more clearly in the manuscript. Showing that Fos increases only in the hemisphere where there is a large CSD-Ca2+ wave is a clear demonstration of this. While Fos increases can certainly be well linked to plasticity in some experimental paradigms, the implication that Fos increases underlie CSD-induced plasticity and possibly therapeutic effects of ECT is not appropriate. Fos increases after CSD are a reliable marker of the very strong neuronal activation that occurs, but Fos increases are not specific for plasticity and can be activated by challenges that do not generate synaptic plasticity. A range of other gene expression changes have been identified with CSD and may contribute to adaptive plasticity; these could be mentioned alongside speculation about Fos. To support the main conclusions of this paper about CSD driving plasticity via Fos, Fos knockout or knockdown studies are needed, as has been used in prior plasticity studies.

https://doi.org/10.7554/eLife.111896.1.sa1

Reviewer #3 (Public review):

Summary:

This manuscript combines widefield calcium imaging, electroencephalography, 2-photon imaging, and immunohistochemistry in mice to re-demonstrate that electroconvulsive stimulation (ECS) induces a seizure followed by cortical spreading depolarization, as previously shown. The putative novel finding - which is not unexpected - is that ECS is also correlated with increased expression of the immediate early gene cFOS, although this has also been shown previously. The authors speculate that CSD drives cFOS expression, which might contribute to the therapeutic effects of ECT; however, experiments performed do not provide causal evidence for this hypothesis. Instead, the authors use expression of cFOS - a nonspecific activity-dependent gene induced in various pathological and non-therapeutic contexts - as a proxy for plasticity and/or therapeutic effect. Hence, overall, the significance of the findings is limited and primarily serves to replicate prior work, with the evidence evaluated as incomplete.

Strengths:

The experiments are generally well executed from a technical perspective.

Main Weaknesses to be addressed in revision:

(1) The main findings of this paper are replication experiments of prior work, and thus, the novelty and significance of this manuscript are relatively limited.

- It is already known that the mean frequency of ECT-induced seizures decays between peak and offset in humans (Stuiver et al. Clin Neurophysiol. 2026 Jan:181:2111439. doi: 10.1016/j.clinph.2025.2111439) and mice (Murakami et al. J Pharmacol Sci 2008 Jan;106(1):78-83. 10.1254/jphs.FP0071453), which the authors re-demonstrate in Figure 1.

- It has already been demonstrated that ECT in mouse models induces lateralized CSD waves in a manner that depends on stimulation parameters and the initial evoked response during stimulation (Rosenthal et al. Nat Comm. 2025 May 18;16(1):4619. doi: 10.1038/s41467-025-59900-1); the authors replicate this in Figures 1, 2, 3, 6.

- It is already widely established that EEG and calcium signals are highly concordant in mouse brain physiology, as shown in Figure 1. It is already known that CSD propagates from supragranular to granular and infragranular layers (Zakharov et al. Epilepsia. 2019 Dec;60(12):2386-2397. doi: 10.1111/epi.16390) as shown in Figure 4.

- It is already known that CSD waves induce cFOS expression (e.g., Dell'Orco et al. Front Cell Neurosci. 2023 Dec 14:17:1292661. doi: 10.3389/fncel.2023.1292661; Hermann and Hossman. Neuroscience. 1999 Jan;88(2):599-608. doi: 10.1016/s0306-4522(98)00249-8) as the authors replicate in Figure 5.

Minimally, the authors should revise claims regarding novelty, as the manuscript, as written, is misleading to a reader not familiar with the field. There is limited innovation in re-demonstrating that these events are seizures and that they involve spreading depolarization.

(2) The authors frame their hypothesis that CSD could be a potential mediator of the therapeutic effects of ECT, but they do not measure therapeutic effects or directly test this hypothesis. The principal advancement of the paper is showing that ECT-induced CSD triggers hemisphere-specific cFOS expression as a proxy of plasticity. However, it is already known that CSD induces cFOS expression (as noted above). The observation that cFOS expression was induced only by CSD, not by the initial seizure, is likely a byproduct of the greater activity induced by CSD than by seizure. cFOS expression is nonspecific to plasticity or therapeutic effects and can be triggered by many non-therapeutic interventions. The cFOS data thus do not meaningfully measure therapeutic plasticity. The authors also selectively cite references

suggesting that EEG metrics such as seizure duration predict positive therapeutic outcomes, but this link is controversial and not well established in the clinical literature.

Minor Weaknesses:

(3) For the n=3 mice used for concurrent 2P imaging with microprism implant, these animals also had ChrimsonR co-expression, but there are no optogenetic studies described in this paper, which is confusing. Yet, this co-expression introduces a significant confound, as GCaMP6 emission (525/50nm band in this study) will overlap substantially with the ChrimsonR excitation spectrum. Thus, the fluorescence emission used to image these neurons may be optogenetically activating them at the same time. Please explain.

(4) Incision of the cortex for implantation of a prism is a significant cortical injury that likely induces CSD instantaneously and may change the propensity for CSD in subsequent recordings. Please comment on this limitation and address how much time elapsed after surgery before imaging.

(5) Method details are missing or insufficiently described for location, titer, and injection strategy for 2-photon experiments.

(6) Given the wide range of parameters used for ECS in mice and ECT in humans, the authors should provide tables for what stimulation parameters were used for each recording. These protocols were chosen manually rather than randomly or systematically, which introduces confounding factors into analyses that use parameters as an independent variable.

(7) While much of the cFOS staining after unilateral CSD shows hemisphere-specific asymmetry, several regions (piriform cortex, amygdala, thalamus) do appear to have bilateral cFOS expression. Please comment on this.

(8) The discussion states: "If CSD accounts for plasticity effects, triggering a CSD in a non-seizure context may be sufficient to elicit therapeutic effects. This is supported by the clinical success of ultra-brief stimulation treatments that do not cause seizures, such as rTMS with accelerated protocols, which achieves treatment efficacy on par with ECT for major depressive disorder". Are the authors implying that TMS induces CSD? What evidence supports this idea?

(9) This statement - "Assuming psychosis is the result of thalamocortical coupling that is too weak in frontal areas of the cortex" (lines 583-585) - may be overly speculative.

https://doi.org/10.7554/eLife.111896.1.sa0